metals

MDPI

Review

Grain Initiation and Grain Refinement: An Overview

Zhongyun Fan * and Feng Gao

Brunel Centre for Advanced Solidification Technology (BCAST), Brunel University, London UB8 3Ph, UK
* Correspondence: zhongyun.fan@brunel.ac.uk

Abstract: Heterogeneous nucleation and grain initiation are two different processes in early-stage solidification (ESS), although both are deterministic. Heterogeneous nucleation refers to the formation of a 2-dimensional (2D) nucleus (a crystal plane of the solid) that can template further growth, while grain initiation is the formation of a hemispherical cap (3D) from which isothermal growth is possible. It is both theoretically and practically beneficial to separate heterogeneous nucleation from grain initiation. This paper provides an overview of our recent understanding of grain initiation behaviour under different conditions and its consequences on grain refinement. After a brief review of the processes involved in the ESS, we present the grain initiation behaviour on a single substrate. This is followed by grain initiation behaviour in systems with a population of nucleant particles with varying particle types (corresponding to varying nucleation undercoolings), where we give detailed descriptions of progressive grain initiation, explosive grain initiation, hybrid grain initiation, grain initiation maps and grain refinement maps. We then provide a brief introduction to the rules that govern competition for heterogeneous nucleation and grain initiation among multiple types of nucleant particles with varying particles' nucleation undercoolings and sizes. Finally, we present the practical implications of grain refinement maps to grain refinement. A key finding from this work is that more significant grain refinement can be achieved by promoting explosive grain initiation using impotent nucleant particles, which is opposite to the traditional approach for grain refinement where potent particles are used to enhance heterogeneous nucleation.

Keywords: solidification; heterogeneous nucleation; grain initiation; grain refinement

Citation: Fan, Z.; Gao, F. Grain Initiation and Grain Refinement: An Overview. *Metals* **2022**, *12*, 1728. https://doi.org/10.3390/met12101728

Academic Editor: Ayrat Nazarov

Received: 1 September 2022
Accepted: 13 October 2022
Published: 15 October 2022

1. Introduction

Grain refinement produces a fine and equiaxed microstructure through solidification processing and is of both scientific and technological importance [1–5]. Scientifically, grain refinement has been a major driving force for developing a scientific understanding of heterogeneous nucleation and is largely responsible for the current status of nucleation science in the metallurgical field, from both positive and negative senses. Technologically, grain refinement not only provides a fine and uniform microstructure for improved materials performance but also offers an effective mechanism for controlling the formation of both second-phase particles and cast defects, both of which are critical factors in determining the performance of materials.

Classical nucleation theory [6–9], denoted as CNT, was based on Gibbs' idea of capillary approximation, and a thermodynamic approach was used to describe the stochastic process of forming a spherical nucleus with a critical radius through balancing the decrease in volume free energy and the increase in interfacial free energy. Statistical mechanics was used to formulae the kinetics of homogeneous nucleation to determine the homogeneous nucleation rate [7,8]. The formulation of homogeneous classical nucleation theory (denoted as homogeneous CNT hereafter) was directly applied later to the heterogeneous nucleation process to describe the spherical cap formation with the same critical radius as in the homogeneous case but with a reduced energy barrier [10,11]. In heterogeneous classical nucleation theory (denoted as heterogeneous CNT hereafter), the contact angle was used as a measure of the nucleation potency of the substrate. Although there have been plenty of

challenges to its validity, CNT has dominated nucleation research for over a century with little significant progress [12].

CNT has so far dictated our scientific understanding of grain refinement, but it has provided little guidance to the practical development of grain refiners [1]. Consequently, the traditional wisdom for grain refiner development is to search for the most potent nucleant particles to enhance heterogeneous nucleation [1,13–16]. This traditional approach is best demonstrated by the development of Al-Ti-B-based grain refiners for grain refining Al-alloys [1–3,17]. Although deploying Al-Ti-B-based grain refiners for grain refining Al-alloys has been a common industrial practice for nearly a century [1,18], the success of these grain refiners is almost an outcome of a trial-and-error approach over many decades [1,18], and the exact mechanism of grain refinement was only elucidated very recently [17]. It is now clear that TiB_2 particles coated with a monoatomic layer of Al_3Ti 2-dimensional compound (2DC) are extremely potent for heterogeneous nucleation of α-Al, while the bare TiB_2 particles are impotent [17].

Although the historical solidification research has been largely concentrated on understanding dendrite formation and its impacts on the evolution of solidification microstructures, the LiME Hub [19] has focused its research on early-stage solidification [20], which includes prenucleation [21–28], heterogeneous nucleation [29–32], spherical cap formation [33], grain initiation [20,34] and spherical growth [35]. It is now clear that although both are deterministic, heterogeneous nucleation and grain initiation are two different processes. Heterogeneous nucleation produces a 2D nucleus (a crystal plane of the solid) that can template further crystal growth, whilst grain initiation provides a hemispherical cap (3D) on a substrate that can grow freely without any energy barrier [29–33]. This has led to the establishment of a three-layer nucleation mechanism [30–32], constrained/unconstrained cap formation processes [33], progressive/explosive grain initiation behaviour and a new approach to grain refinement by deploying impotent nucleant particles to impede nucleation [20,34].

In this paper, we provide a comprehensive overview of grain initiation behaviour under different conditions. Following a brief introduction, Section 2 introduces the concept of early-stage solidification to put grain initiation into a wider context; in Section 3, we describe heterogeneous nucleation and grain initiation processes on a single substrate; Section 4, the main body of the paper, offers a comprehensive account of grain initiation behaviour in the systems containing a group of nucleant particles with varying particle sizes; Section 5 describes the basic rules of competition for heterogeneous nucleation and grain initiation among different types of nucleant particles with varying particles sizes. This is followed by a discussion on the implications of grain initiation behaviour on grain refinement before a brief summary.

2. Early-Stage Solidification (ESS) and Grain Initiation

According to their unique characteristics and their consequences for the final solidified microstructure, the solidification processes of metallic materials can be divided into three distinctive stages: early-stage solidification (ESS), middle-stage solidification (MSS) and last-stage solidification (LSS). ESS dictates grain structures and macro-segregation, MSS determines grain morphology and micro-segregation and LSS affects the formation of second-phase particles and casting defects. Whilst the historical solidification research has been mainly focused on MSS, particularly on dendritic growth, the LiME Hub research has been concentrated on ESS. As shown in Figure 1, ESS was defined by Fan [20,34] as a solidification process that occurs in the time interval between the onset of melt cooling and the morphological instability of growing solid particles [36–38], which often coincides with recalescence under solidification conditions relevant to industrial practice. ESS covers prenucleation, heterogeneous nucleation, spherical cap formation, grain initiation and spherical growth. In this section, we briefly introduce these processes to put grain initiation into a wider context.

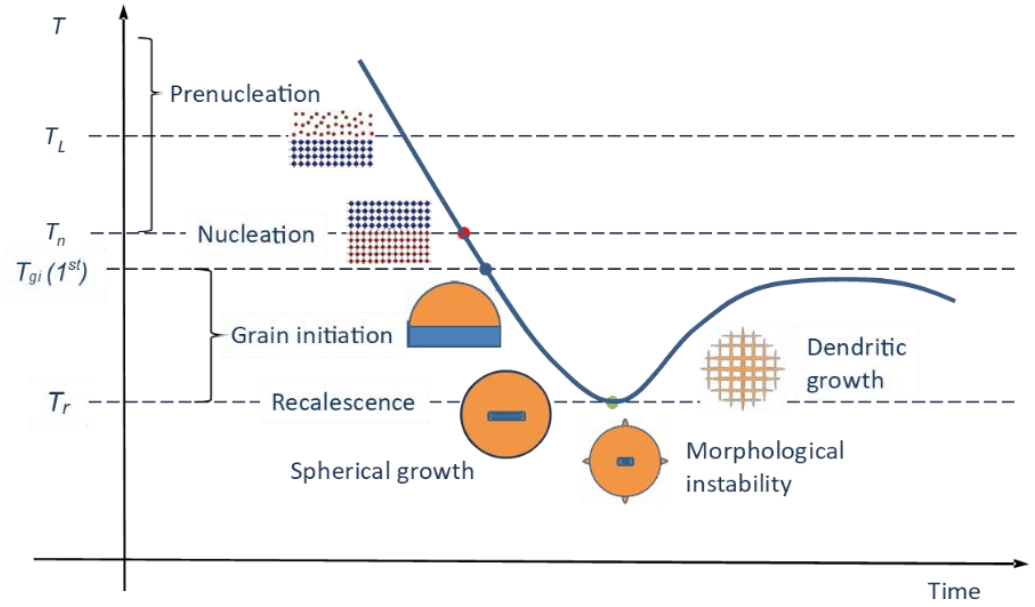

Figure 1. A schematic cooling curve illustrating the solidification processes by following a specific nucleant particle, which has initiated a grain in the solidified microstructure [20,34]. Please note that the length scale of the sketches increases with time following the solidification processes.

Prenucleation refers to the phenomenon of substrate-induced atomic ordering in the liquid adjacent to the liquid/substrate interface at temperatures above the nucleation temperature [21,28]. Prenucleation is manifested by atomic layering normal to the interface and in-plane atomic ordering parallel to the interface [21]. Extensive atomistic simulations have confirmed that prenucleation is favoured by a decreased lattice misfit between the solid and substrate [21], a reduced atomic level surface roughness [22] and an enhanced attractive interaction between the substrate and the liquid [23]. Prenucleation can be manipulated by the chemical segregation of selected elements at the liquid/substrate interface [17,39,40], such as Ti at the Al(l)/TiB_2 interface to enhance nucleation [17] and Ti and Zr at the Al(l)/TiB_2 interface to impede nucleation [40]. Prenucleation reaches its maximum at the nucleation temperature and provides a precursor for heterogeneous nucleation [33].

Heterogeneous nucleation was recently described by Fan et al. [30–33] as an atomistic process that produces a 2D nucleus (i.e., a crystal plan of the solid) by building on the precursor provided by prenucleation. The 2D nucleus can then template further growth. The heterogeneous nucleation process can be generally described as a three-layer mechanism and is schematically illustrated in Figure 2 [33] and will be described in more detail in the next section. It should be pointed out that the 3-layer heterogeneous nucleation mechanism generates a 2D nucleus, while the classical heterogeneous nucleation produces a 3D nucleus from which the solid phase may grow [30–33]. In fact, in the new description of early-stage solidification, the classical heterogeneous nucleation (cap formation) has been redefined as grain initiation.

Spherical cap formation is a process that follows heterogeneous nucleation but before the formation of a hemisphere on the substrate, as depictured in Figure 3 [33]. After nucleation, further growth will lead to the development of curvature at the liquid/solid interface, which may become a constraint to further growth depending on the relative position of nucleation undercooling (ΔT_n) and the grain initiation undercooling (ΔT_{gi}) (Figure 4) [33]. When $\Delta T_n < \Delta T_{gi}$, the curvature becomes a constraint growth, further undercooling is required to overcome an energy barrier and the spherical cap formation is hence constrained. In this case, the heterogeneous nucleus (2D) and the cap cover the entire substrate surface. However, when $\Delta T_n > \Delta T_{gi}$, there is no energy barrier to further growth, and the cap formation is unconstrained, as illustrated in Figure 4a. In this case,

the heterogeneous nucleus (2D) and the spherical cap only cover a patch of the substrate surface. It is clear from Figure 4b that there is an energy barrier for the constrained cap formation, while the unconstrained cap formation is barrier-less (or downhill).

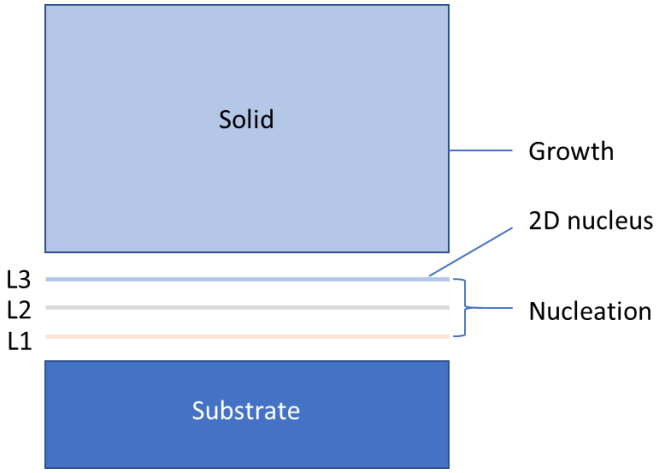

Figure 2. Schematic illustration of the 3-layer nucleation mechanism [33]. At the nucleation temperature, heterogeneous nucleation starts with a precursor created by the prenucleation, proceeds layer-by-layer through a structural templating mechanism, and completes within 3 atomic layers (marked as L1, L2 and L3) to provide a 2D nucleus (L3, a crystal plane of the solid) which can template further growth of the solid.

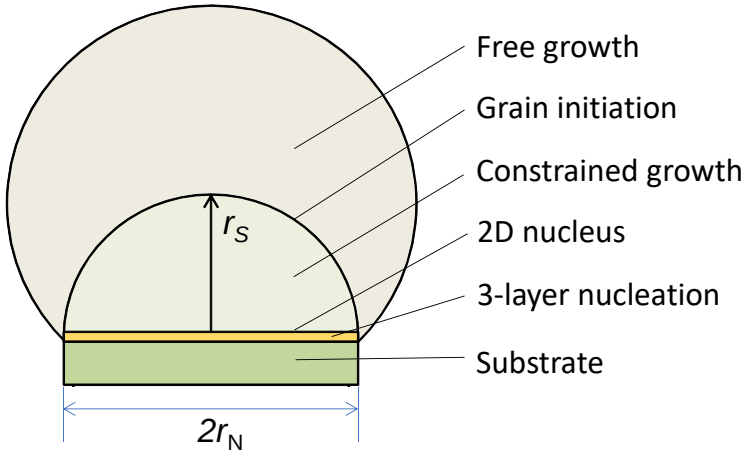

Figure 3. Schematic diagram of heterogeneous nucleation, cap formation and grain initiation [33]. Please note that the sizes of the nucleation and cap formation are not on the same scale.

Grain initiation concerns whether a solid particle can grow isothermally at a given temperature. Grain initiation is governed by the free growth criterion [20,41], which describes a critical condition where the spherical cap becomes a hemisphere (i.e., $r_S = r_N$, where r_S and r_N are the radii of the solid and the substrate, respectively) (Figure 3). If $\Delta T < \Delta T_{gi}$, the solid will remain as a cap (dormant) and further undercooling is required for further growth, while if $\Delta T > \Delta T_{gi}$, the solid can grow freely without any energy barrier, which has been referred to as free growth in the literature [41]. It should be pointed out that grain initiation is whether a solid particle (substrate covered with solid), not a substrate, can grow freely although the free growth criterion is described as a function of substrate size.

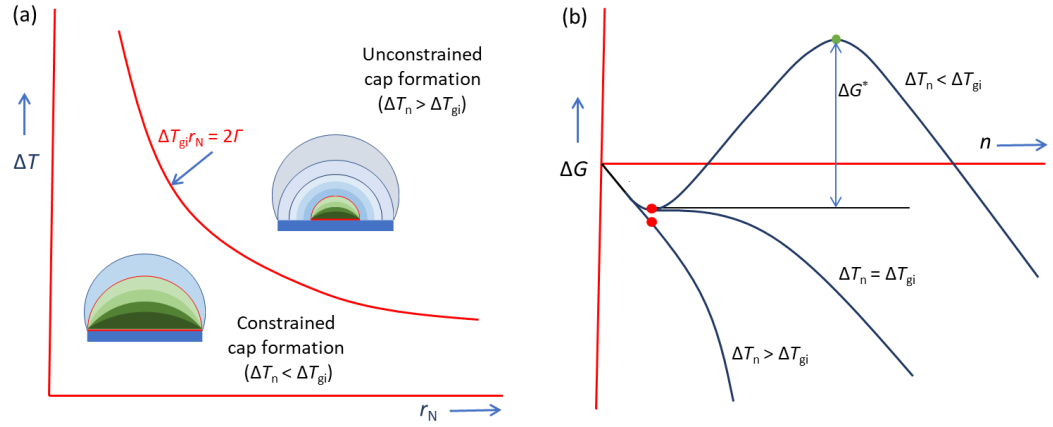

Figure 4. Schematic illustration of (**a**) grain initiation behaviour on a single substrate and (**b**) change in Gibbs free energy during the grain initiation process [33]. The free growth criterion, $\Delta T_{gi} r_N = 2\Gamma$ (the solid red line in (**a**)), divides the $\Delta T_{gi} - r_N$ plot into two regions: I, where $\Delta T_{gi} r_N > 2\Gamma$, grain initiation has no energy barrier and occurs through unconstrained cap formation, and II, where $\Delta T_{gi} r_N < 2\Gamma$, grain initiation has an energy barrier and occurs through constrained cap formation. The red dot in (**b**) represents the onset of cap formation, and the green dot marks the onset of grain growth.

3. Heterogeneous Nucleation and Grain Initiation on a Single Substrate

3.1. Classical Nucleation Theory

Based on the capillarity approximation, homogeneous CNT describes a stochastic process for the formation of a critical nucleus (a 3D solid cluster with a critical size r^*), where an atomic cluster with a radius r and $r < r^*$ (an embryo) will dissolve into the melt, while a cluster with $r \geq r^*$ (a nucleus) will grow [12]. The thermodynamic approach was used to determine the critical radius of the nucleus (r^*) and the nucleation energy barrier (ΔG^*) by balancing the volume free-energy change and the interfacial free-energy change [12]:

$$\Delta G = -\frac{4}{3}\pi r^3 \Delta G_v + 4\pi r^2 \gamma_{LS} \tag{1}$$

$$r^* = \frac{2\gamma_{LS}}{\Delta G_v} \tag{2}$$

$$\Delta G^* = \frac{16\pi\gamma_{LS}^3}{3(\Delta G_v)^2} \tag{3}$$

where ΔG is the total free-energy change for the formation of a solid cluster with a radius of r, ΔG_v is the free-energy change for solidification per unit volume and γ_{LS} is the interfacial free energy of the liquid/solid interface. On the right-hand side of Equation (1), the first term is the volume free-energy change, and the second term is the interfacial free-energy change.

Statistical mechanics was used to describe the nucleation rate [7,8]. Although there have been challenges to the validity of capillarity approximation [42], homogeneous CNT is conceptually simple and mathematically rigorous and has therefore dominated our way of handling nucleation for over a century. As will be shown later, homogeneous CNT is also compatible with the framework of early-stage solidification.

Directly applying the formulation of homogeneous CNT to the case of heterogeneous nucleation has established the heterogeneous CNT. Heterogeneous CNT predicts that although the critical nucleus radius is the same for both homogeneous and heterogeneous nucleation, the critical energy barrier for heterogeneous nucleation is reduced compared with that for homogeneous nucleation due to the presence of the substrate. Heterogeneous

CNT uses the contact angle, θ, to describe the potency of a substrate for heterogeneous nucleation, and θ is defined by Young's equation [43] as follows:

$$\gamma_{LN} = \gamma_{SN} + \gamma_{LS}\cos\theta \tag{4}$$

where γ_{LN}, γ_{SN} and γ_{LS} are the interfacial energies for the liquid/substrate, solid/substrate and liquid/solid interfaces, respectively. A precondition for θ to be valid is that $\gamma_{LN} < \gamma_{SN} + \gamma_{LS}$. However, the recent molecular dynamics (MD) simulations have confirmed that heterogeneous nucleation is a spontaneous process (a downhill process) and that in all the 3-layer nucleation cases, we have [32]:

$$\gamma_{LN} > \gamma_{SN} + \gamma_{LS} \tag{5}$$

Therefore, it is concluded that heterogeneous CNT is invalid [32]. This is somewhat not surprising for the following reasons. Firstly, it is now widely accepted that heterogeneous nucleation is a deterministic process [29–32]; the direct application of a stochastic homogeneous CNT to describe a deterministic process is too much of a stretch. Secondly, during the spherical cap formation process, θ increases with increasing cap height, and therefore, θ is an ill-defined parameter for measuring the nucleation potency of the substrate. Finally, but not least, there have been frequent challenges to the validity of heterogeneous CNT in the literature. For instance, Cantor and co-workers [42,44,45] pointed out that when $\theta < 10^{\circ}$, heterogeneous CNT becomes unphysical, and the kinetics of CNT are inaccurate for efficient catalysis at low undercooling.

3.2. A 3-Layer Nucleation Mechanism of Heterogeneous Nucleation

Upon the realization of the invalidity of heterogeneous CNT, Fan and co-authors systematically investigated the heterogeneous nucleation process at the atomic level using MD simulation [30,31,33]. They found that heterogeneous nucleation is a deterministic process that occurs spontaneously at the nucleation temperature and completes within the first 3 atomic layers to produce a 2D nucleus for templating further growth [30,31,33]. The heterogeneous nucleation process can be generally summarized as a three-layer mechanism (Figure 2). The specific atomistic mechanism within the three atomic layers during nucleation is closely related to the sign and amplitude of the lattice misfit (f) between the substrate and the solid. For systems with a small negative misfit ($-12.5\% < f < 0$), the first atomic layer (L1) accommodates the misfit by the formation of an edge dislocation network, the second atomic layer (L2) reduces the lattice distortion by twisting a small angle through the formation of a screw dislocation network and the third atomic layer (L3) is the 2D nucleus (a crystal plane of the solid). For systems with a small positive misfit ($0 < f < 12.5\%$), L1 is epitaxy to the substrate surface, L2 accommodates misfit by the formation of vacancies and L3 is the 2D nucleus. However, for systems with a large misfit ($|f| > 12.5\%$), prenucleation will produce a new substrate surface that is a coincident site lattice (CSL) to the original substrate surface; the CSL accommodates the majority of the misfit (f_{CSL}), leaving a small residual misfit (f_{r}). The exact atomistic mechanism for heterogeneous nucleation will be determined by the nature of f_{r}; if $f_{\mathrm{r}} < 0$, the dislocation mechanism will apply; otherwise, a vacancy mechanism will operate if $f_{\mathrm{r}} > 0$.

The three-layer mechanism has been used to formulating heterogeneous nucleation, and we derived the following equations for nucleation undercooling [32,33]:

$$\Delta T_n = \frac{|\Delta\gamma|}{12\Delta f_s \Delta S_v r_a} \tag{6}$$

$$\Delta\gamma = \gamma_{LS} + \gamma_{SN} - \gamma_{LN} \tag{7}$$

where Δf_s is the difference in solid atom fraction in the nucleation system after and before the 3-layer nucleation, ΔS_v is the entropy of fusion per unit volume and r_a is the atomic radius of a solid atom. The three-layer nucleation theory predicts implicitly that nucleation

undercooling increases linearly with the increase in lattice misfit [32,33], and this is in good agreement with Turnbull's crystallographic theory [46] and Fan's epitaxial nucleation theory [29].

3.3. Free Growth of a Nucleated Solid Particle

After nucleation, the 2D nucleus can potentially template further growth of the solid, leading to the formation of a spherical cap on the substrate with a specified curvature at the liquid/solid interface. The curvature may become a constraint to further growth during the cap formation process, depending on the relative positions of nucleation undercooling (ΔT_n) and grain initiation undercooling (ΔT_{gi}) [33], where ΔT_{gi} is defined by the free growth criterion [20,41] derived from the CNT:

$$\Delta T_{gi} r_N = 2\Gamma \tag{8}$$

$$\Gamma = \gamma_{LS} / \Delta S_v \tag{9}$$

where Γ is the Gibbs–Thompson coefficient, which is a material constant of the solidifying system. In Equation (8), ΔT_{gi} defines the undercooling required for the spherical cap to become a hemisphere where the volume energy term and the interfacial energy term are balanced ($\Delta G = 0$ in Equation (1)).

As schematically illustrated in Figure 4, when $\Delta T_n > \Delta T_{gi}$, the volume energy term dominates the cap formation process, there is no energy barrier and the cap formation process is unconstrained. However, when $\Delta T_n < \Delta T_{gi}$, the interfacial energy term dominates the cap formation process, and the cap formation becomes a constrained process. In the latter case, a spherical cap can only grow to a curvature specified by the given undercooling. Further growth of the cap requires an increase in undercooling. In both constrained and unconstrained cap formation processes, the solid particle will be able to freely grow once the cap grows beyond the hemisphere, i.e., the solid particle can grow isothermally without an energy barrier. Under such conditions, we say that a grain has been initiated. Both constrained and unconstrained cap formation refer to the growth process before grain initiation, while free growth refers to the growth process after grain initiation, as schematically illustrated in Figure 3.

It becomes clear that the spherical cap formation process described in the heterogeneous CNT should be treated as grain initiation rather than heterogeneous nucleation. Grain initiation concerns whether a solid particle can grow freely and is only relevant to the size of the substrate, while heterogeneous nucleation is strongly dependent on the physical and chemical nature of the substrate.

4. Grain Initiation Behaviour of a Population of Solid Particles

Nucleant particles in an actual melt have a range of sizes that follows a log-normal size distribution [47,48]. The grain initiation behaviour of these particles is strongly dependent on the chemical and physical nature of the nucleant particles, the alloy composition and the solidification conditions [20]. In this section, we present our latest understanding of grain initiation behaviour in systems containing a population of nucleant particles of varying particle sizes. The results were mainly obtained by numerical modelling [20] using the parameters listed in Table 1 [20,47,49].

4.1. Progressive Grain Initiation (PGI)

Progressive grain initiation (PGI) is defined as a process of grain initiation, which starts with the largest particle(s) at $\Delta T_{gi}(1^{st})$, continues progressively with the smaller ones and finishes at recalescence, as schematically depictured in Figure 5a [20,34]. A necessary condition for progressive grain initiation is $\Delta T_n < \Delta T_{gi}(1^{st})$, i.e., heterogeneous nucleation takes place before any grain initiation event. PGI occurs during the solidification processing of engineering alloys containing very potent nucleant particles (both in situ and ex situ).

Table 1. The main parameters used in the numerical calculation [20,47,49].

Parameters (Symbol, Unit)	Al-Cu	Mg-Al
Partition coefficient (k)	0.13 [49]	0.37 [20]
Liquidus slope (m, K(wt pct)$^{-1}$)	−2.5 [49]	−6.87 [20]
Heat capacity (c_{pv}, Jm^{-3}K^{-1})	2.58×10^6 [47]	2.59×10^6 [20]
Enthalpy of fusion (ΔH_V, Jm^{-3})	9.5×10^8 [47]	6.75×10^8 [20]
Diffusion coefficient (D, m^{2}s^{-1})	2.52×10^{-9} [47]	2.7×10^{-9} [20]
Gibbs-Thompson coefficient (Γ, Km)	1.42×10^{-7} [47]	1.48×10^{-7} [20]
Volume (V_0, m^3)	1×10^{-6}	1×10^{-6}
Cooling rate (K/s)	3.5	3.5

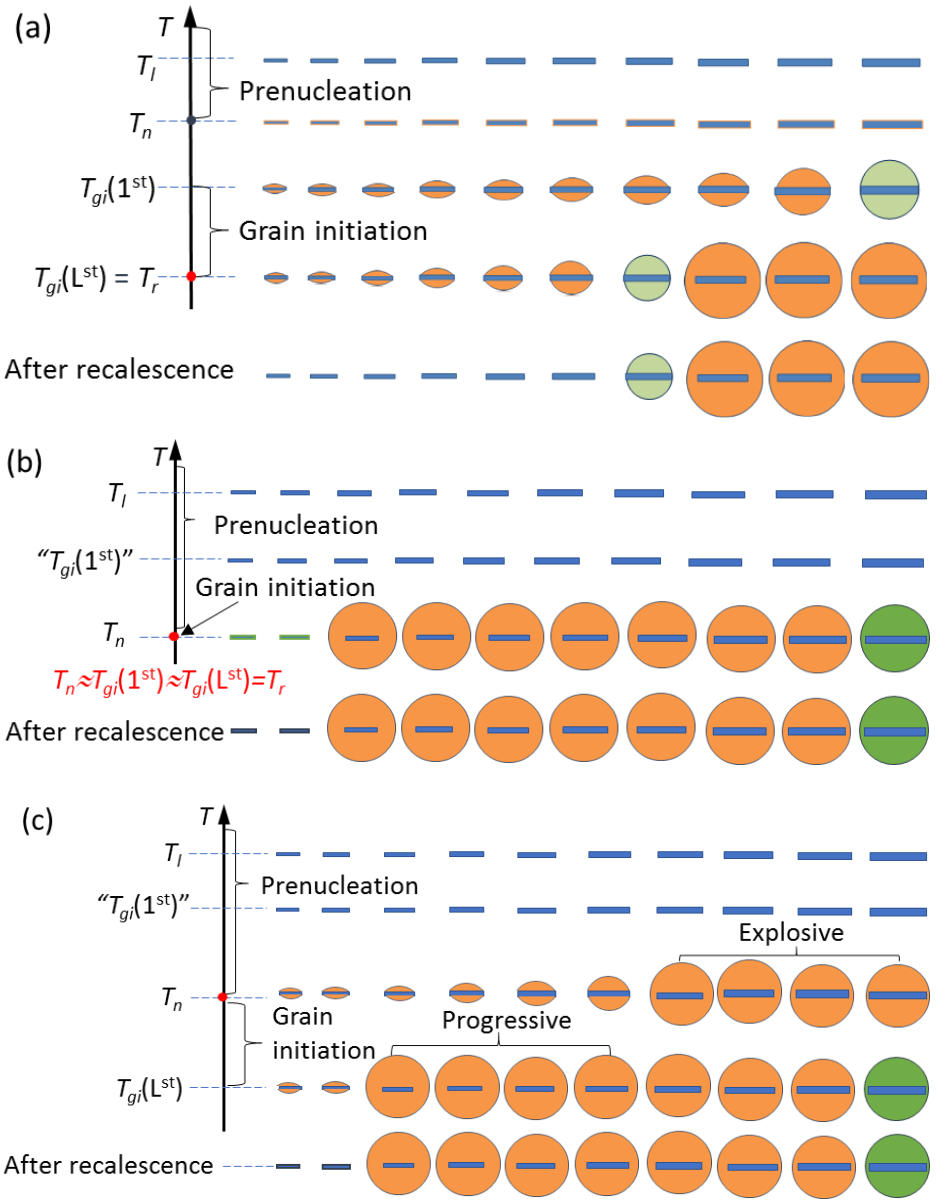

Figure 5. Schematic illustration of grain initiation behaviour during solidification of metallic alloys [20,34]. (**a**) Progressive grain initiation (PGI) occurs when nucleation occurs before any grain initiation event ($\Delta T_n < \Delta T_{gi}(1^{st})$); (**b**) explosive grain initiation (EGI) occurs when nucleation causes immediate recalescence ($\Delta T_n = \Delta T_{max}$ ($T_L - T_r$)); (**c**) hybrid grain initiation (HGI) occurs firstly with some EGI events followed by some PGI events ($\Delta T_{gi}(1^{st}) \leq \Delta T_n < \Delta T_{gi}(L^{st})$).

We take the solidification process of Al-1Cu alloy as an example to illustrate PGI. The Al-1Cu alloy is inoculated with 1 ppt (0.1 wt.%) of Al-5Ti-1B grain refiner and solidifies at a cooling rate ($\dot{T}$) of 3.5 K/s. The TiB_2 particles in the alloy melt have a number density of $N_0 = 7.3 \times 10^{12}$ m^{-3}, a log-normal size distribution with a geometrical mean particle size of $d_0 = 0.68$ μm and a standard deviation of $\sigma = 0.876$ [47], and a nucleation undercooling of $\Delta T_n = 0.01$ K [41] to reflect the extremely high nucleation potency of TiB_2/Al_3Ti-2DC particles [17]. This solidification condition is similar to that of DC (direct chill) casting of Al-alloys with grain refiner addition.

To conduct numerical simulations, we need to work out the size of the largest nucleant particle, $d(1^{st})$ and its corresponding grain initiation undercooling $\Delta T_{gi}(1^{st})$. Both $d(1^{st})$ and $\Delta T_{gi}(1^{st})$ are functions of d_0, σ, N_0 and the total volume (assumed to be 1 cm^3 here). The calculated $d(1^{st})$ and $\Delta T_{gi}(1^{st})$ for Al-1Cu alloy with TiB_2 particles are shown in Figure 6a as a function of particle number density. For a given type of nucleant particles with a log-normal size distribution, $d(1^{st})$ increases and $\Delta T_{gi}(1^{st})$ decreases with increasing particle number density.

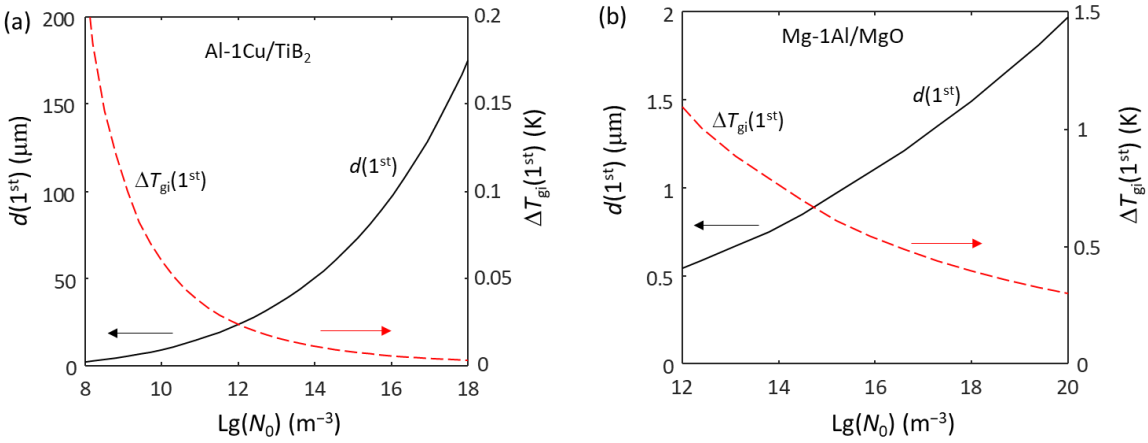

Figure 6. The calculated size of the largest nucleant particle ($d(1^{st})$) and its corresponding free growth undercooling $\Delta T_{gi}(1^{st})$ as a function of the total number density of nucleant particles (N_0, m^{-3}). (**a**) Al-1Cu alloy inoculated by commercial Al-5Ti-1B grain refiner; and (**b**) Mg-1Al alloy containing native MgO particles.

PGI manifests itself in the cooling curve by the gradual reduction of the cooling rate to 0 at recalescence. The calculated cooling curve for Al-1Cu alloy inoculated by 1 ppt Al-5Ti-1B grain refiner at a cooling rate of 3.5 K/s is shown in Figure 7a. At recalescence, the maximum undercooling ΔT_{max} is 0.21 K, the solid fraction is 2.63×10^{-4} and the average solid particle size (diameter at recalescence) is 10.5 μm. The predicted final grain size (d_g) is 105 μm from the final grain number density at recalescence, N_g, by the following equation [41]:

$$d_g = \left(\frac{0.5}{N_g}\right)^{1/3}. \quad (10)$$

Another key feature of PGI is that the instantaneous grain initiation rate ($\dot{N}$, i.e., number of grain initiation events per unit volume per unit time) initially increases and then decreases with time due to the latent heat released by the growing initiated grains, finally reaching zero at the recalescence point (Figure 7b). Consequently, the cumulative grain initiation events normalised by the total number density of TiB_2 particles (N/N_0) increases with time and becomes a constant, showing a maximum after recalescence (Figure 7b). After recalescence, there is no more grain initiation due to the rise in temperature. The total duration for grain initiation is 0.08 s, and the maximum number density of initiated grains is 4.26×10^{11} m^{-3}, which represents 5.8% of the total number density of the TiB_2 particles.

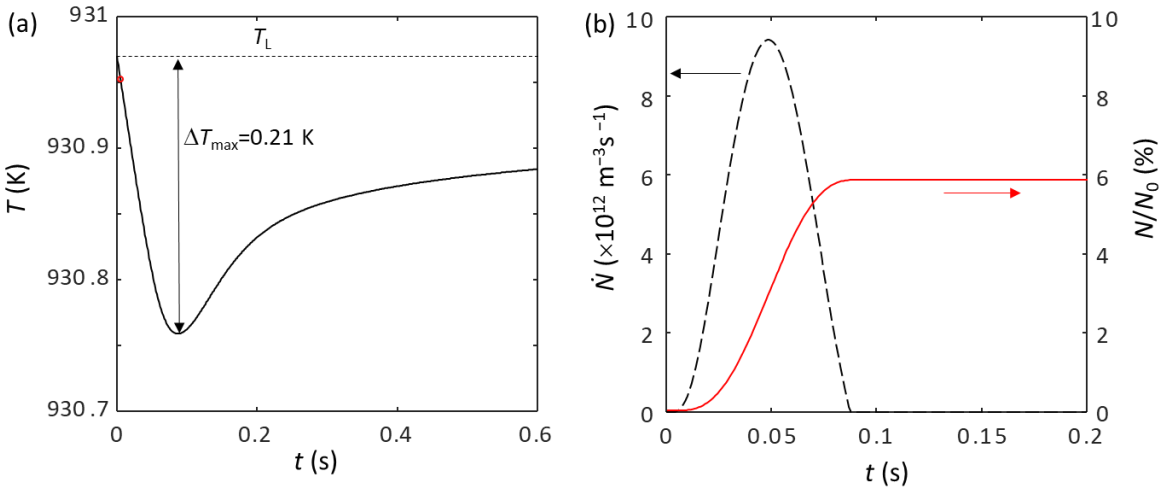

Figure 7. (**a**) Calculated cooling curve of Al-1Cu alloy and (**b**) the instantaneous grain initiation rate ($\dot{N}$) and accumulative grain initiation events per unit volume (N) normalised by the total number density of TiB_2 particles (N_0), showing the progressive grain initiation behaviour during solidification of Al-1Cu alloy inoculated by 1 ppt Al-5Ti-1B grain refiner ($N_0 = 7.3 \times 10^{12}$ m^{-3}) at a cooling rate of 3.5 K/s. The red dot in (**a**) marks the onset of grain initiation.

In this specific case of PGI, heterogeneous nucleation takes place with a small undercooling ΔT_n (assumed to be 0.01 K) on all available TiB_2 particles coated with Al_3Ti 2DC. The largest TiB_2 particle(s), $d(1^{st})$, is 33 μm, which corresponds to a grain initiation undercooling ($\Delta T_{gi}(1^{st}) = 0.017$ K) that is larger than ΔT_n, suggesting that the grain initiation process is a typical PGI. The last grain initiation event occurs on particle(s) of $d(L^{st}) = 2.7$ μm at $\Delta T_{gi}(L^{st}) = \Delta T_{max} = 0.21$ K. After recalescence, all the solid particles that failed to initiate grains will dissolve back into the melt due to the rise in temperature.

4.2. Explosive Grain Initiation (EGI)

Explosive grain initiation (EGI) is defined as a grain initiation process in which a group of solid particles initiate grains almost simultaneously and the latent heat released by both heterogeneous nucleation and the initial free growth can cause an immediate recalescence which stifles any further grain initiation events [20,34]. Figure 5b schematically illustrates the explosive grain initiation process during the solidification of alloys containing only relatively impotent nucleant particles [20,34]. "$\Delta T_{gi}(1^{st})$" marks the undercooling at which the largest particle should free-grow if heterogeneous nucleation has occurred. When the undercooling (ΔT) is between "$\Delta T_{gi}(1^{st})$" and ΔT_{max} (the undercooling at recalescence), many solid particles have satisfied the free growth criterion and should free-grow if heterogeneous nucleation has occurred. At ΔT_n, heterogeneous nucleation occurs on all nucleant particles, and this is followed immediately by simultaneous grain initiation on those particles which have satisfied the grain initiation criterion and cause recalescence instantly. Heterogeneous nucleation, grain initiation and recalescence all occur in an extremely short time interval, and consequently, we have $\Delta T_n \approx \Delta T_{gi}(1^{st}) \approx \Delta T_{gi}(L^{st}) \approx \Delta T_{max}$. Similar to the case of PGI, after recalescence, all the solid particles that failed to initiate grains will dissolve back into the melt.

Here we use Mg-1Al alloy containing native MgO particles as an example to illustrate the EGI process. The total number density of the MgO particles is set at 10^{17} m^{-3} with a log-normal size distribution ($d_0 = 0.07$ μm, $\sigma = 0.45$) [50], the cooling rate is set at 3.5 K/s, and the nucleation undercooling is estimated to be $\Delta T_n = 1.2$ K [20] reflecting the low nucleation potency of MgO [24,51,52]. This solidification condition is similar to that of the DC casting of Mg alloys with intensive melt shearing [50]. The $d(1^{st})$ and $\Delta T_{gi}(1^{st})$ for Mg-1Al alloy with native MgO particles are calculated and shown in Figure 6b. The largest particle $d(1^{st})$

is 1.28 μm, corresponding to a grain initiation undercooling of "$\Delta T_{gi}(1^{st})$" = 0.46 K, being smaller than ΔT_n (1.2 K).

The most significant feature of EGI manifested in the cooling curve is the constant cooling rate before recalescence and a sharp rise in temperature after recalescence. The calculated cooling curve of the Mg-1Al alloy is shown in Figure 8a. In contrast to Figure 7a, the calculated cooling curve exhibits a very sharp rise in temperature immediately after recalescence. The maximum undercooling ΔT_{max} is 1.2 K, which is the ΔT_n for MgO, indicating this is a typical EGI. At recalescence, the solid fraction is 7.6×10^{-5} and the predicted final grain size is 88 μm.

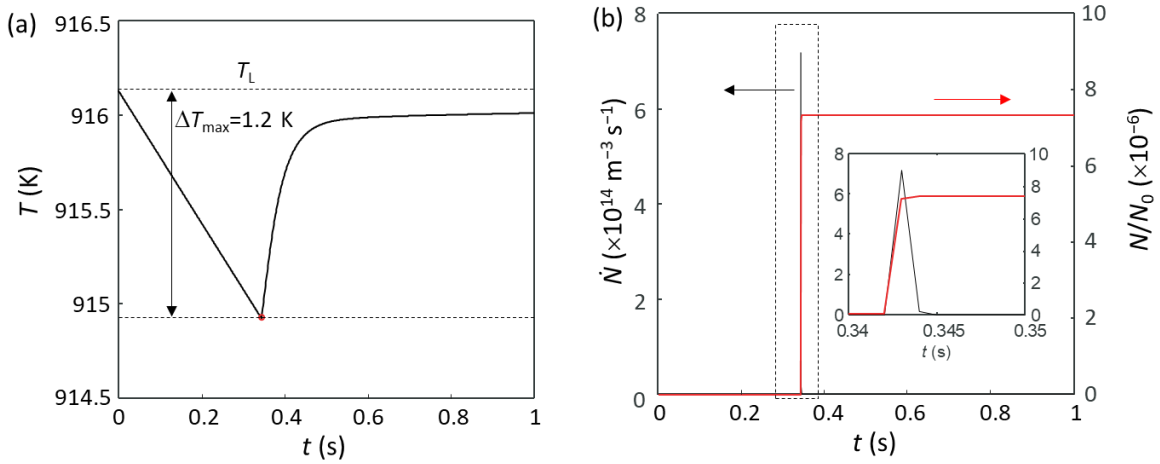

Figure 8. (**a**) Calculated cooling curve of Mg-1Al alloys and (**b**) the instantaneous grain initiation rate ($\dot{N}$) and accumulative grain initiation events per unit volume (N) normalised by the total number density of MgO particles (N_0), showing the explosive grain initiation behaviour during solidification of Mg-1Al alloy containing native MgO particles ($N_0 = 10^{17}$ m^{-3}) at a cooling rate of 3.5 K/s. The red dot in (**a**) marks the onset of grain initiation. The insert in (**b**) shows a magnified view of the area marked in the dotted box.

Both instantaneous grain initiation rate ($\dot{N}$) and cumulative grain initiation events per unit volume normalised by the total number density of MgO particles (N/N_0) increase almost vertically with time (Figure 8b). The maximum number density of initiated grains is 7.33×10^{11} m^{-3}. The insert in Figure 8b with a finer time scale shows that grain initiation occurs in an extremely short time interval. This suggests that grain initiations take place explosively, with the instantaneous grain initiation rate being in the order of 10^{14} s^{-1}m^{-3}.

In this case, heterogeneous nucleation can only take place at larger undercooling ΔT_n on all available MgO particles. Although many MgO particles with a particle size between 0.11 μm and 1.3 μm satisfied the free growth criterion at smaller undercooling, grain initiation can only occur at larger undercooling after nucleation. However, at such great undercooling, many solid particles are ready to free-grow almost simultaneously causing an immediate recalescence, which stifles any further grain initiation by the remaining solid particles with a smaller size.

4.3. Hybrid Grain Initiation (HGI)

Hybrid grain initiation (HGI) is defined as a grain initiation process in which a group of large nucleant particles initiate grains simultaneously in an explosive manner, and this is followed by progressive grain initiation on smaller nucleant particles until recalescence, as depictured in Figure 5c. A necessary condition for HGI is $\Delta T_{gi}(1^{st}) < \Delta T_n < \Delta T_{max}$ [20]. In this case, once the nucleation occurs, these solid particles that satisfy the free growth criterion will initiate grains in an EGI manner. However, the amount of latent heat released is not sufficient to cause recalescence. Further cooling of the melt leads to further grain initiation in a PGI manner until recalescence.

Here we take the solidification process of Mg-1Al alloy containing a hypothetical type of nucleant particles (ΔT_n = 1.0 K) as an example to illustrate HGI. The total number density of the nucleant particles is set at 10^{17} m^{-3} with a log-normal size distribution (d_0 = 0.07 μm, σ = 0.45), and the cooling rate is set at 3.5 K/s.

The calculated cooling curve and grain initiation rate are shown in Figure 9 [20]. As ΔT_n = 1.0 K is larger than $\Delta T_{gi}(1^{st})$ (0.46 K), when the temperature decreases to T_n, heterogeneous nucleation takes place on all the nucleant particles, this is followed by simultaneous grain initiation on those nucleated particles that have satisfied the grain initiation criterion. However, the amount of latent heat released from those grain initiation events cannot compensate for the heat extracted by the environment, and then the temperature will continue to decrease until recalescence. During this period, smaller solid particles will continue to initiate grain in a progressive manner (Figure 9b).

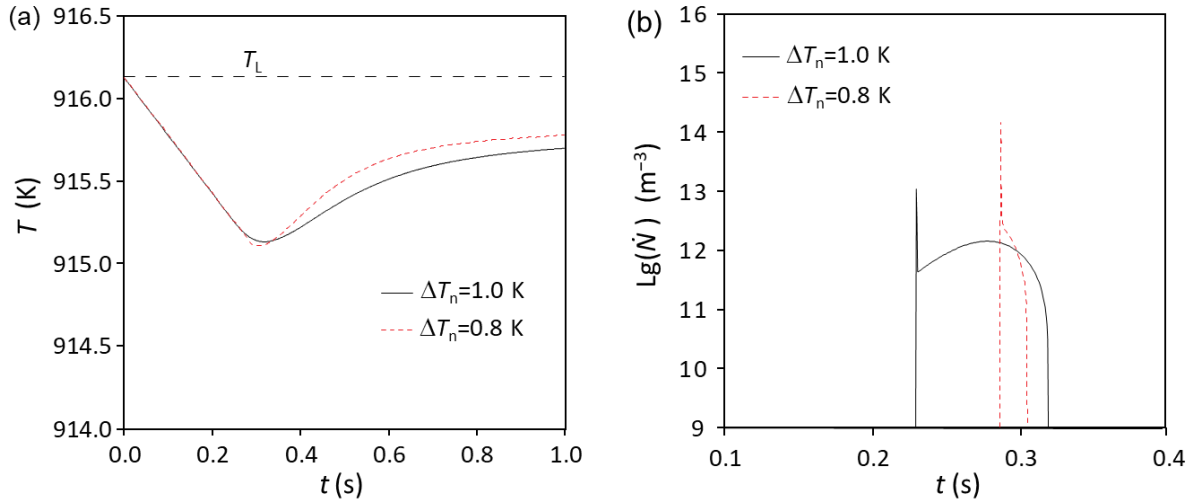

Figure 9. (**a**) Calculated cooling curve of Mg-1Al alloy and (**b**) the instantaneous grain initiation rate ($\dot{N}$) during solidification of Mg-1Al alloy containing artifical particles with ΔT_n = 1.0 K and ΔT_n = 0.8 K with the same particle number density and size distribution as native MgO particles ($N_0 = 10^{17}$ m^{-3}, d_0 = 0.07 μm, σ = 0.45) at a cooling rate of 3.5 K/s [20].

The maximum undercooling ΔT_{max} is 1.02 K in this case, which is very close to the nucleation undercooling (1.0 K). At recalescence, the solid fraction is 1.83×10^{-4} and the predicted final grain size is 157 μm. In addition, EGI events account for 81.5% of the total grain initiation events, indicating that EGI events dominate the grain initiation process.

For comparison, we also investigated the grain initiation behaviour during the solidification of Mg-1Al alloy containing hypothetical nucleant particles with ΔT_n = 0.8 K. In this case, the maximum undercooling ΔT_{max} becomes 0.99 K, being slightly higher than ΔT_n (0.8 K). At recalescence, the solid fraction is 4.92×10^{-4} and the predicted final grain size is 176 μm. EGI events only account for 8.9% of the total grain initiation events, indicating that the PGI events dominate the grain initiation process.

4.4. Grain Initiation Maps

In this section, we explore the relationships between PGI, HGI and EGI through understanding the effect of the nucleant particles (ΔT_n and N_0), alloy compositions (C_0) and solidification conditions (e.g., $\dot{T}$) on grain initiation behaviour. It should be noted that ΔT_n is used as a measure of nucleation potency of the nucleant particles, and hence different values for ΔT_n represent different types of nucleant particles. For this purpose, we developed the concept of the grain initiation map [20], which describes the grain initiation behaviour under different conditions. Figure 10 shows a schematic grain initiation map in the form of the $\Delta T_n - \dot{T}$ plot to introduce the basic features of a grain initiation map. There are two boundary lines and a triple point that divide the $\Delta T_n - \dot{T}$ plot into

three zones: PGI, EGI and HGI zones. The PGI/HGI boundary line (blue) represents $\Delta T_n = \Delta T_{gi}(1^{st})$; the EGI/HGI boundary line represents $\Delta T_n = \Delta T_{gi}(L^{st})$; and the triple point represents $\Delta T_n = \Delta T_{gi}(1^{st}) = \Delta T_{gi}(L^{st}) = \Delta T_{max}$. Each of these grain initiation zones has its own unique characteristics: (1) progressive grain initiation zone: $\Delta T_n < \Delta T_{gi}(1^{st})$; (2) explosive grain initiation zone: $\Delta T_n = \Delta T_{max}$; and (3) hybrid grain initiation zone: $\Delta T_{gi}(1^{st}) \leq \Delta T_n < \Delta T_{gi}(L^{st})$. In addition, there is a triple point that links the 3 zones, which represents a special case of grain initiation. Solidification at the triple point is characterised by $\Delta T_n = \Delta T_{gi}(1^{st}) = \Delta T_{max}$. Physically, it means that immediately after heterogeneous nucleation, grain initiation on the largest solid particle(s) triggers recalescence. Therefore, grain initiation at the triple point is EGI. Furthermore, as will be shown later, grain initiation maps can also take the form of $\Delta T_n - C_0$ and $\Delta T_n - N_0$ plots. Finally, the largest particle, $d(1^{st})$, is determined by the particle number density, particle size distribution and the volume of the melt. This means that $\Delta T_{gi}(1^{st})$ is a function of particle characteristics and melt volume and should be independent of the cooling rate and solute concentration. That is the reason why the $\Delta T_n = \Delta T_{gi}(1^{st})$ is a vertical line in the grain initiation map.

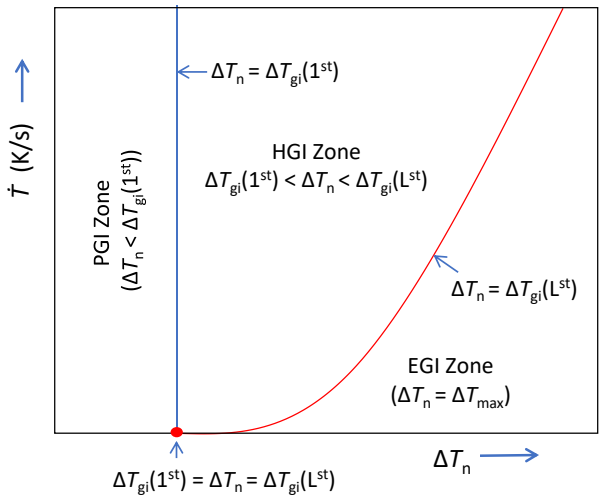

Figure 10. Schematic illustration of the grain initiation map presented as a $\dot{T} - \Delta T_n$ plot. The blue line represents the bounder between PGI and HGI zones; the red line marks the bounder between HGI and EGI zones; the red dot is the triple point between the PGI, HGI and EGI zones.

Now we use the solidification of Mg-Al alloys containing hypothetical nucleant particles of varying nucleation potency (ΔT_n) as an example to illustrate the basic features of grain initiation maps. The established grain initiation maps for Mg-Al alloys with varying ΔT_n are presented in Figure 11 in the form of $\Delta T_n - \dot{T}$ (Figure 11a), $\Delta T_n - C_0$ (Figure 11b) and $\Delta T_n - N_0$ (Figure 11c) plots to assess the effect of particle nucleation potency, cooling rate, solute concentration, and particle number density on grain initiation behaviours [20]. The grain initiation maps (Figure 11) suggest that EGI is generally promoted by decreasing nucleation potency (increasing ΔT_n), solute concentration and cooling rate but increasing particle number density. On the opposite, PGI is favoured by increasing particle nucleation potency, cooling rate, solute concentration and decreasing particle number density.

To further demonstrate the effect of particle number density on grain initiation behaviour, we calculated the grain initiation maps for Mg-10Al alloy containing nucleant particles with a constant particle size distribution but with varying nucleation potency and two different particle number densities (10^{15} m^{-3} and 10^{17} m^{-3}). The results are shown in Figure 12. The grain initiation map for $N_0 = 10^{15}$ m^{-3} is shown by the solid blue lines and that for $N_0 = 10^{17}$ m^{-3} by the dashed red lines. With the increase in particle number density from 10^{15} m^{-3} to 10^{17} m^{-3}, the EGI zone expands significantly at the expense of mainly the HGI zone and to a certain extent the PGI zone. Therefore, it can be concluded that increasing particle number density is very effective to promote EGI.

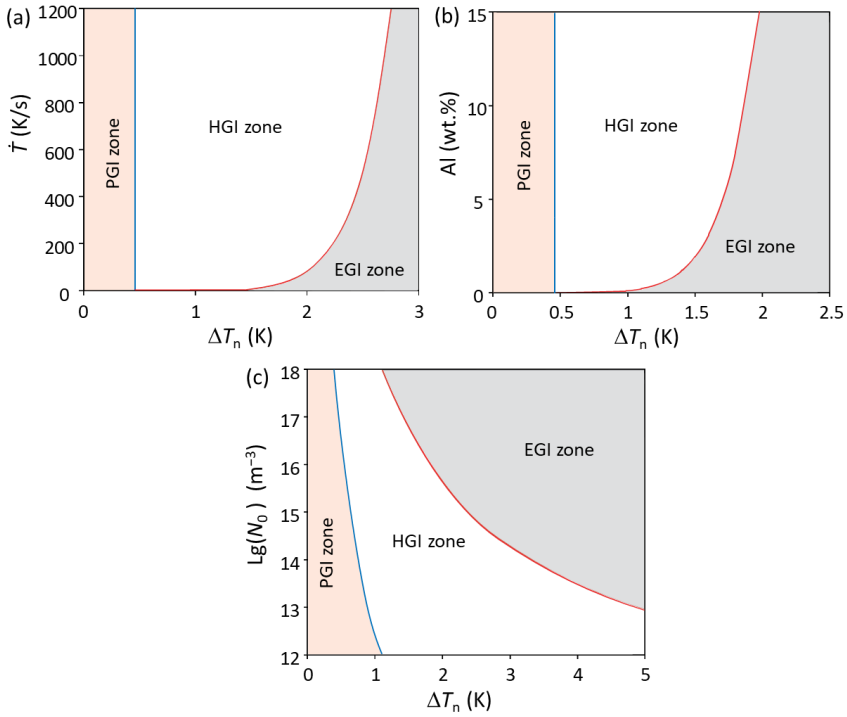

Figure 11. Grain initiation maps for Mg-Al alloys containing nucleant particles with varying nucleation potency but constant log-normal particle size distribution [20]. (**a**) Grain initiation map ($\Delta T_n - \dot{T}$ plot) for Mg-1Al alloy with $N_0 = 10^{17}$ m^{-3} showing the effect of cooling rate on grain initiation behaviour; (**b**) grain initiation map ($\Delta T_n - C_0$ plot) for Mg-Al alloys with $N_0 = 10^{17}$ m^{-3} and $\dot{T}$ = 3.5 K/s showing the effect of solute concentration on grain initiation behaviour; (**c**) grain initiation map ($\Delta T_n - N_0$ plot) for Mg-1Al alloy with $\dot{T}$ = 3.5 K/s showing the effect of particle number density on grain initiation behaviour. The solid blue line marks the limit for progressive grain initiation ($\Delta T_n = \Delta T_{gi}(1^{st})$) and the red line marks the limit for explosive grain initiation ($\Delta T_n = \Delta T_{max}$). These two lines divide the grain initiation map into 3 distinct zones: the progressive grain initiation zone (PGI) where $\Delta T_n < \Delta T_{gi}(1^{st})$; the explosive grain initiation zone (EGI) where $\Delta T_n = \Delta T_{max}$; and the hybrid grain initiation zone (HGI) where $\Delta T_{gi}(1^{st}) \leq \Delta T_n < \Delta T_{max}$.

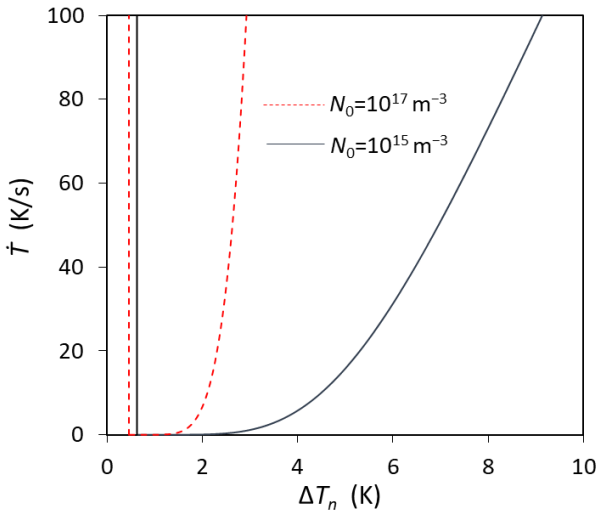

Figure 12. Calculated grain initiation maps for Mg-10Al alloy inoculated by nucleant particles with varying nucleation potency, different particle number densities (10^{15} m^{-3} and 10^{17} m^{-3}) but the same log-normal size distribution (d_0 = 0.07 μm, σ = 0.45). It suggests that EGI is promoted by increasing the number density of nucleant particles.

Figure 13 shows the three superimposed grain initiation maps for Mg-Al alloys with three different compositions containing nucleant particles with varying nucleation potency but with constant particle size distribution and number density ($N_0 = 10^{17}$ m^{-3}). Due to the constant number density, all three maps have the same PGI/HGI boundary line. Figure 13 suggests that decreasing alloy composition expands the EGI zone but does not affect the PGI zone.

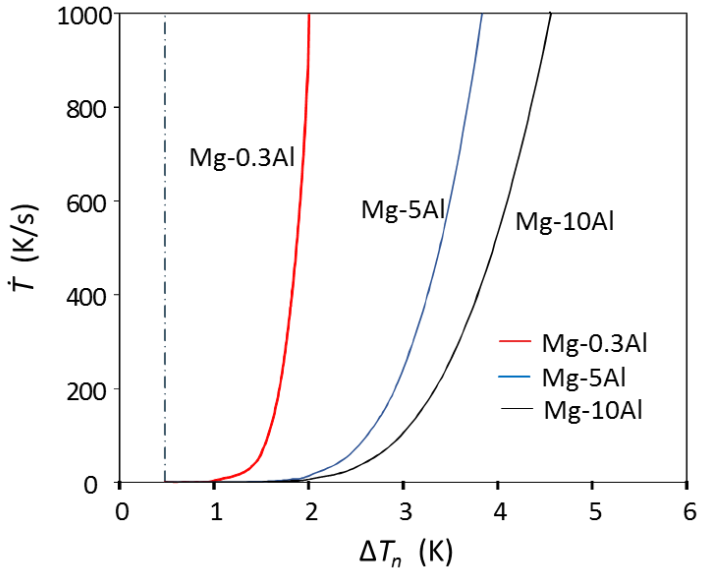

Figure 13. Calculated grain initiation maps for Mg-Al alloy with different solute contents inoculated by nucleant particles which have the same log-normal size distribution and the same particle number density ($N_0 = 10^{17}$ m^{-3}) but varying nucleation potency. It shows that EGI is favoured by decreasing solute concentration.

4.5. Grain refinement maps

One of the primary objectives of solidification modelling is to predict the grain size of cast microstructures solidified under different conditions. To understand the effect of grain initiation behaviour on grain size, we developed the concept of grain refinement maps [20]. Using the iso-grain-size lines, we established the contour of grain size variation in the $\Delta T_n - \dot{T}$, $\Delta T_n - C_0$ and $\Delta T_n - N_0$ plots. Figure 14 schematically illustrates a grain refinement map in the form of the $\Delta T_n - \dot{T}$ plot. The solid line represents the situation where the numbers of EGI (N_{EGI}) and PGI (N_{PGI}) events are equal, i.e., $N_{\mathrm{EGI}}/N_{\mathrm{PGI}} = 1$. This solid line divides the $\Delta T_n - \dot{T}$ plot into two distinctive regions, PGI dominant zone where $N_{\mathrm{EGI}}/N_{\mathrm{PGI}} < 1$ and EGI dominant zone where $N_{\mathrm{EGI}}/N_{\mathrm{PGI}} > 1$. The dashed line represents the iso-grain-size line, on which the grain size produced under different conditions is constant. A series of such iso-grain-size lines will form a landscape of grain size as functions of parameters relevant to solidification, which can then be used as a guide for grain refinement.

The effects of particle nucleation potency, particle number density, cooling rate and solute concentration on grain size are demonstrated by the grain refinement maps in Figure 15 [20]. It can be seen from Figure 15a,b that the cooling rate and solute concentration have a similar trend in the grain size. In the PGI-dominant zone, grain size decreases with increasing cooling rate and solute concentration but is almost independent of ΔT_n for a given cooling rate and solute concentration; in contrast, in the EGI-dominant zone, grain size decreases with increasing ΔT_n but is almost independent of cooling rate and solute concentration for a given ΔT_n. However, for a given ΔT_n, the grain size decreases with increasing particle number density in both the PGI-dominant zone and EGI-dominant zone (Figure 15c).

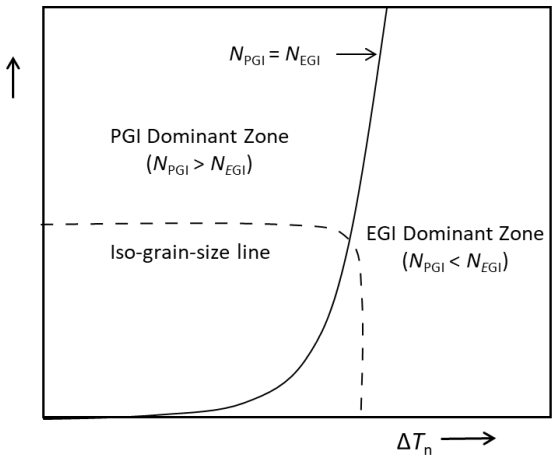

Figure 14. Schematic illustration of the grain refinement map presented as a $\dot{T} - \Delta T_n$ plot. The solid line represents a condition where PGI and EGI have the equal number of events ($N_{\mathrm{PGI}} = N_{\mathrm{EGI}}$). It divides the $\dot{T} - \Delta T_n$ plot into the PGI dominate zone ($N_{\mathrm{PGI}} > N_{\mathrm{EGI}}$) and the EGI dominate zone ($N_{\mathrm{PGI}} < N_{\mathrm{EGI}}$).

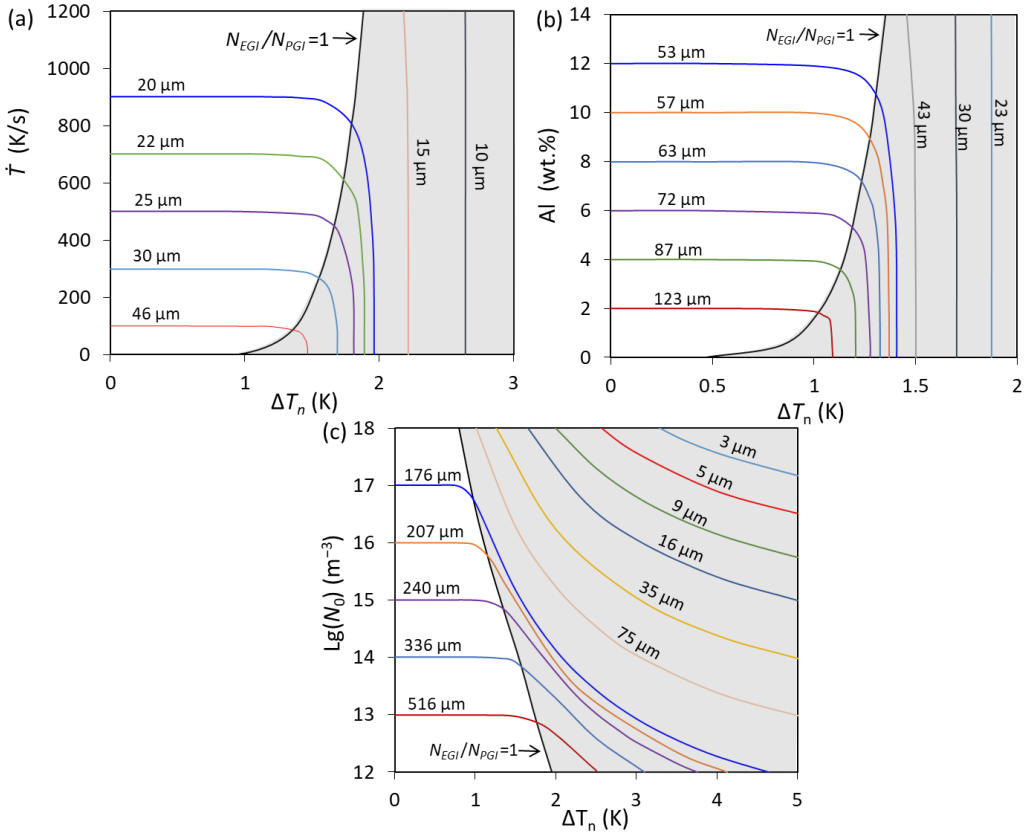

Figure 15. Grain refinement maps for Mg-Al alloys containing nucleant particles with varying nucleation potency but constant log-normal particle size distribution [20]. (**a**) Grain refinement map ($\Delta T_n - \dot{T}$ plot) for Mg-1Al alloy with $N_0 = 10^{17}$ m^{-3} showing the effect of cooling rate on grain refinement; (**b**) grain initiation map ($\Delta T_n - C_0$ plot) for Mg-Al alloys with $N_0 = 10^{17}$ m^{-3} and $\dot{T} = 3.5$ K/s showing the effect of solute concentration on grain refinement; (**c**) grain initiation map ($\Delta T_n - N_0$ plot) for Mg-1Al alloy with $\dot{T} = 3.5$ K/s showing the effect of particle number density on grain refinement. The solid black line represents a condition where EGI has equal proportion with PGI ($N_{\mathrm{EGI}}/N_{\mathrm{PGI}} = 1$); the white and grey coloured zones mark PGI-dominant and EGI-dominant zones, respectively. The thin coloured lines represent iso-grain-size lines.

We analysed the grain size dependence of Mg-Al alloys on solute concentration (C_0), cooling rate ($\dot{T}$) and particle number density (N_0) under different grain initiation behaviours, and the results are presented in Figure 16 [20]. From Figure 16, the following conclusions can be drawn: (1) EGI is more effective for grain refinement than PGI; (2) for fully PGI, grain size decreases with increasing solute concentration, cooling rate and particle number density; (3) for fully EGI, grain size is independent of solute concentration and cooling rate but decreases slightly with increasing particles number density; and (4) for HGI, grain size decreases with increasing solute concentration, cooling rate and particle number density, and the decrease in grain size is more pronounced in the EGI-dominant zone than in the PGI-dominant zone with increasing particle number density.

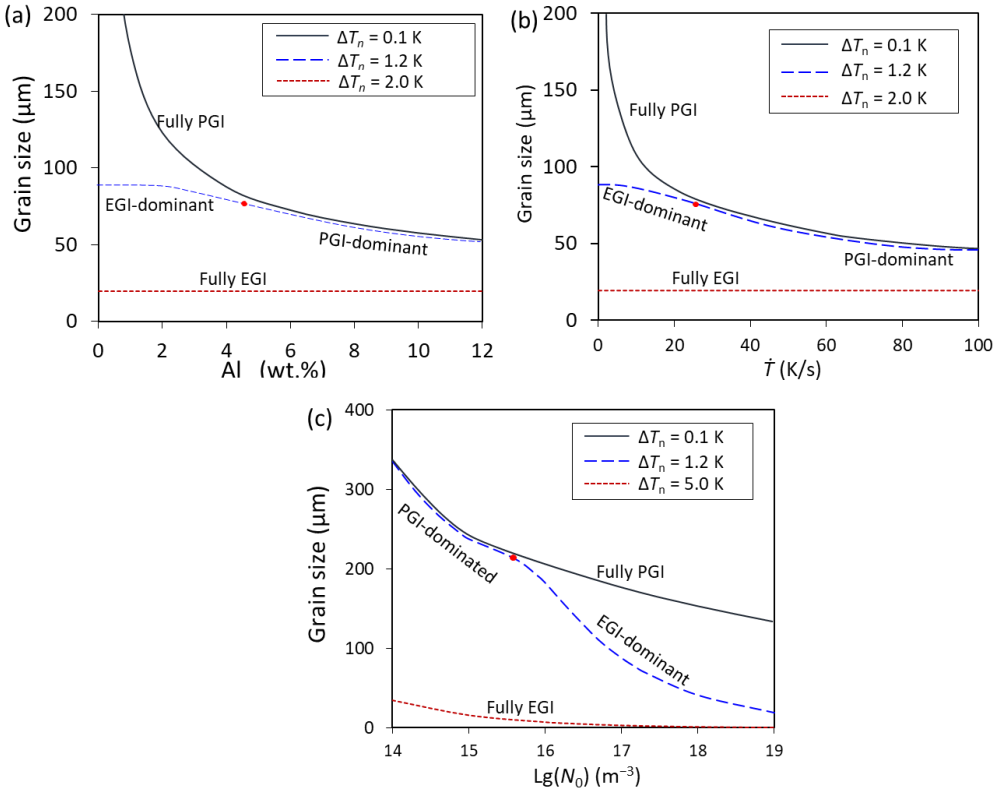

Figure 16. Grain size dependence of Mg-Al alloys on (**a**) solute concentration (C_0), (**b**) cooling rate ($\dot{T}$), and (**c**) particle number density (N_0) under different grain initiation behaviours [20]. The constant values are used for the following parameters: C_0 = 1% (Al); $N_0 = 10^{17}$ m^{-3}; d_0= 0.07 μm; σ = 0.45; and $\dot{T}$ = 3.5 K/s. The nucleation potency (ΔT_n) is varied to ensure grain initiation behaviour is either fully PGI (solid blue line), fully EGI (dotted red line) or typical HGI (dashed blue line). The red dot represents the condition of $N_{EGI} = N_{PGI}$.

In addition, further insights on grain refinement can be obtained from the grain refinement maps in Figure 15 and parameter analysis in Figure 16:

- For a given alloy (fixed C_0) containing potent nucleant particles (small ΔT_n and thus more likely PGI) with a specified casting process (fixed $\dot{T}$), the addition of more potent nucleant particles (smaller ΔT_n) will not lead to further grain refinement (Figure 15a,b). This means that the nucleant particles for chemical inoculation need to be just more potent than the native particles to dominate the heterogeneous nucleation and grain initiation processes, but not more potent than that.
- When EGI is dominant, grain refinement is independent of solute concentration and cooling rate (Figure 15a,b). In this case, further grain refinement can be achieved by increasing particle number density (Figure 15c) and decreasing particle potency (i.e., increasing nucleation undercooling).

- When multiple types of nucleant particles with multiple particle sizes are present in the melt, EGI delivers much more significant grain refinement than PGI does (Figures 15 and 16). Thus, under this condition, any factor that promotes EGI will lead to more grain refinement.

5. Grain Initiation Behaviour in Systems with Different Types of Nucleant Particles

We established in Section 3 the grain initiation behaviour on a single substrate and in Section 4 the grain initiation behaviour in systems containing a population of nucleant particles of the same chemical nature. We found that the basic principles governing grain initiation behaviour are closely related to the interplay between nucleation undercooling (ΔT_n) and grain initiation undercooling (ΔT_{gi}). In this section, we lay down the basic rules for grain initiation behaviour in systems containing more than one type of nucleant particle.

Alloy melts relevant to industrial practice usually contain more than one type of nucleant particle. They can be both endogenous particles (e.g., oxides, nitrides, carbides, and borides) and exogenous (e.g., grain refiner particles and other entrained inclusions). These coexisting nucleant particles may have a range of nucleation potency, particle number density and size distribution, leading to a complex situation where all the particles compete for both heterogeneous nucleation and grain initiation. Fan and coworkers [53,54] have investigated both experimentally and theoretically heterogeneous nucleation and grain initiation in such complex systems and established the basic rules that govern such competitions. They found that the competition is governed by two basic rules, one for heterogeneous nucleation and one for grain initiation [54]. The competition for heterogeneous nucleation is governed by [54]:

$$\Delta T_n = Min\{\Delta T_n(i)\} \tag{11}$$

where $\Delta T_n(i)$ is the nucleation undercooling of the ith type of nucleant particle. Heterogeneous nucleation is a deterministic process and is independent of particle size. It occurs first on nucleant particles with the smallest nucleation undercooling and then progressively on particles with larger nucleation undercooling. This continues until recalescence, which denies the chances for heterogeneous nucleation on these particles that have not nucleated so far.

Competition for grain initiation only occurs on these particles that have participated in heterogeneous nucleation. Once nucleation occurred, there will be solid caps on those substrates. Although the free growth criterion relates grain initiation undercooling with the substrate size (Equation 8), grain initiation concerns whether a solid particle can freely grow to initiate a grain, which is independent of the nature of the substrate, such as misfit, surface roughness and chemistry. Therefore, competition for grain initiation is among all those solid particles and is irrelevant to the substrates from which the solid particles were nucleated in the first place. According to the free growth criterion [20,41], we have the following competition rule for grain initiation [54]:

$$\Delta T_{gi} = Max\{r_N(i)\} \tag{12}$$

where $r_N(i)$ is the radius of the ith nucleant particles that have participated in heterogeneous nucleation. Equation (12) states that among all the solid particles largest solid particles initiate grain first followed by grain initiation on progressively smaller ones regardless of which type of nucleant particles they were nucleated in the first place.

This competition rule for grain initiation is schematically illustrated in Figure 17 [54]. In a hypothetical melt containing three different types of nucleant particles (denoted as A, B and C) with their unique size distributions. It is also assumed that all three types of nucleant particles have participated in heterogeneous nucleation (i.e., $\Delta T_n(i) \leq \Delta T_{\max}$). Also shown in Figure 17 is their corresponding grain initiation undercooling. If the maximum achievable undercooling (e.g., limited by recalescence) is $\Delta T_{\max}$ and its corresponding minimum substrate size is $r_{\min}$, only nucleant particles with $r_N \geq r_{\min}$ can initiate grains. This means

that all the C particles and some of the B particles can initiate grains, whilst all the A particles will not participate in grain initiation.

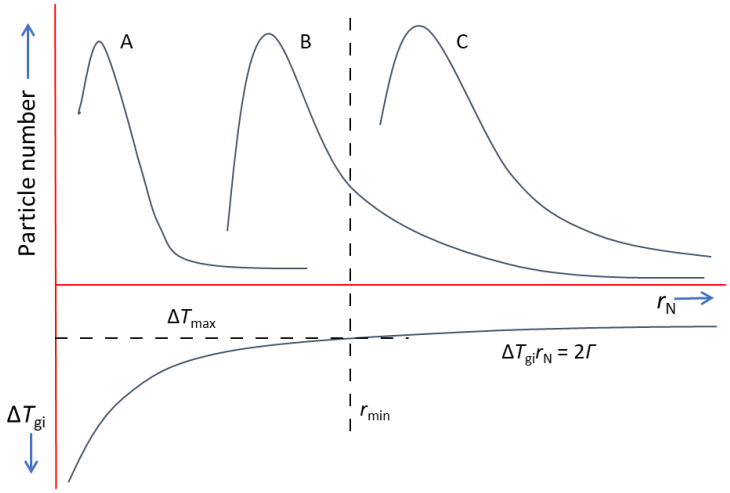

Figure 17. Schematic illustration of the competition for grain initiation with 3 different types of nucleant particles, A, B and C, which have different particle sizes and size distributions [54].

6. Implications for Grain Refinement

6.1. TiB_2-Based Grain Refiners Have Reached Their Limit for Grain Refinement

The traditional wisdom regarding achieving grain refinement dictates enhancing heterogeneous nucleation by the addition of potent nucleant particles (i.e., to reduce ΔT_n) to alloy melts prior to solidification, for example, grain refining Al-alloys by the addition of TiB_2-based grain refiners [1], such as Al-5Ti-1B master alloy, which includes plenty of TiB_2/Al_3Ti-2DC particles with extremely high nucleation potency for nucleating α-Al. Based on this principle, some new grain refiners have been developed for Al alloys [55–58] and Mg alloys [59–63].

Although the exact mechanism of the heterogeneous nucleation of TiB_2-based grain refiners was only understood recently [17], such grain refiners have been optimized in terms of their performance by trial and error over the last 80 years. It appears that there is very little space for further improvement of their performance [47]. In this section, we analyse the performance of TiB_2-based grain refiner in view of the new framework of heterogeneous nucleation and grain initiation and identify approaches for more effective grain refinement.

One possible approach is to increase nucleation potency by replacing the TiB_2 particles with more potent nucleant particles. Figure 18a shows the predicted grain sizes of Al-1Cu alloy inoculated by hypothetical nucleant particles with varying nucleation potency but with a constant particle number density ($N_0 = 10^{13}$ m^{-3}) and particle size distribution ($d_0 = 0.67$ µm and $\sigma = 0.876$). Figure 18a suggests that the addition of more potent nucleation particles or making TiB_2 more potent than TiB_2/Al_3Ti-2DC will promote PGI and will not lead to further grain refinement, or even increase grain size. This means that any attempt to develop grain refiners by using nucleant particles more potent than TiB_2/Al_3Ti-2DC may have little chance to be successful.

Another possible approach is to increase TiB_2 particle number density. Grain refinement can be achieved in commercial purity Al alloy (CP-Al) with the addition of 3.5×10^{12} m^{-3} TiB_2 particles (about 0.5 ppt addition of Al-5Ti-1B grain refiner), where the microstructure changes from columnar to equiaxed [64]. However, after columnar-to-equiaxed transition (CET), further addition of TiB_2 particles could not significantly reduce the grain size in CP-Al alloy [64], which agrees with the calculations as shown in Figure 18b, where the calculated grain size of Al-1Cu alloy at $\dot{T} = 3.5$ K/s is plotted against the level of TiB_2 addition. In Figure 18b, it can be seen that the calculated grain size only reduces from

148 μm to 70 μm when the N_0 of TiB_2 particles increases from 10^{12} m^{-3} to 10^{15} m^{-3}, 3 orders of magnitude increase in particle number density, or equivalently, 0.1 to 10 wt.% grain refiner addition, which is not making any practical sense.

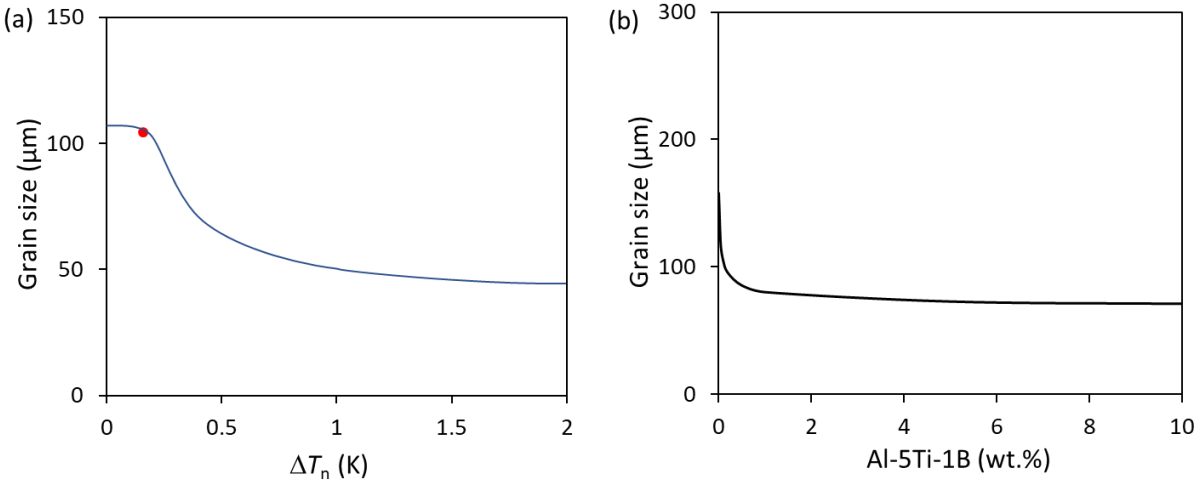

Figure 18. The predicted grain size of Al-1Cu alloy inoculated by (**a**) hypothetical nucleant particles with varying nucleation potency but with a constant particle number density ($N_0 = 10^{13}$ m^{-3}) and particle size distribution (log-normal with $d_0 = 0.67$ μm and $\sigma = 0.876$), (**b**) different levels of addition of Al-5Ti-1B grain refiner. The red dot in (**a**) marks $N_{PGI} = N_{EGI}$.

Yet another possible approach is to alter TiB_2 particle size and/or size distribution. Like any other particles grown naturally from a chemical reaction process, TiB_2 particles have a log-normal size distribution ($d_0 = 0.67$ μm and $\sigma = 0.876$) [47]. Theoretically, for a fixed level of grain refiner addition (fixed weight percent), decreasing d_0 (equivalent to increasing particle number density) and reducing σ (narrowing size distribution), particularly using mono-sized particles and eliminating the large particles in the tail of particle size distribution, can all potentially increase the total number of grain initiation events and thus decrease grain size. However, none of these approaches is easily achievable in practice. Therefore, it can be concluded that it is not practical to deliver grain refinement by altering the particle size distribution.

A further possible approach is to reduce the level of agglomeration of TiB_2 particles in the grain refiner. It has been confirmed both theoretically and experimentally that particle agglomeration reduces the number of grain initiation events and ultimately leads to larger grain size since only one particle (the largest one) can initiate a grain among all the particles in an agglomerate [65]. However, the TiB_2 particles in the grain refiner rods are already dispersed to a large extent by extensive deformation processing during the rod production process. It seems that little space is left for the improvement of particle dispersion in a practical sense. Based on the above analysis, we can conclude that after over 80 years of development by trial and error, the current TiB_2-based grain refiners are highly optimized for grain refinement of Al-alloys, leaving little space for further development. To deliver more significant grain refinement, new approaches are required.

6.2. Native MgO Particles Offer a Great Opportunity for Grain Refinement of Mg-Alloy

Compared with TiB_2 particles in the well-known TiB_2-based grain refiners [17], native MgO particles in Mg alloys offer a number of distinctive characteristics with respect to grain refinement [20,50], such as an order of magnitude smaller mean particles size (70 nm vs. 700 nm for d_0), a narrow size distribution (0.45 vs. 0.88 for σ), 4 orders of magnitude larger particle number density (10^{17} m^{-3} vs. 10^{13} m^{-3} for N_0) and more importantly, larger nucleation undercooling (1.2 K vs. 0.01 K for ΔT_n). All these characteristics can be made in favour of grain refinement.

In Mg-alloy melts, MgO is the only type of particle of significance to grain refinement although other types of particles do exist. Due to its high oxidation potential, molten magnesium oxidizes readily and rapidly when it is in contact with air, resulting in the formation of magnesium oxide (MgO) and magnesium nitrides (Mg_3N_2) [66,67]. In addition, MgS and MgF_2 may also form through the reaction of molten Mg with protective gases [66,67]. However, among these and other inclusions, MgO particles are the dominant inclusions in Mg alloys in terms of particle number density. Although other inclusion particles may participate in heterogeneous nucleation or even grain initiation, their existence will not alter significantly neither the general features of solidification processes nor the final grain size due to their low number density in Mg-melts. Therefore, we can conclude that native MgO is the only type of particle of significance in Mg-alloy melts in terms of grain refinement.

Native MgO particles have two different types of morphology, octahedral MgO with {111} surface termination (denoted as MgO{111}) and cubic MgO with {001} surface termination (denoted as MgO{001}), although MgO{111}) particles are dominant in numbers [52]. MgO{111} particles have a log-normal size distribution with a small geometric mean diameter (d_0 = 0.07μm) and a mall standard deviation (σ = 0.45) [50,52]. However, most of the native MgO particles are present in the alloy melt in the form of oxide films that can be effectively dispersed using intensive melt shearing [50,68], making the effective number density as high as 10^{17} m^{-3} [50]. Small particle size, narrow size distribution, being amenable to dispersion by high shear and very high number density make native MgO very suitable for grain refinement of Mg-alloys.

Native MgO particles are highly impotent for the heterogeneous nucleation of Mg [24,50–52,68]. The lattice misfit between MgO and α-Mg is 7.86% for both MgO{111} and MgO{100} substrates [52], which is much larger than that between Zr and α-Mg (0.9% [53]) and that between TiB_2/Al_3Ti-2DC (0.09% [17]). In addition, density functional theory (DFT) calculations have confirmed that both MgO{111} and MgO{100} substrates are atomically rough due to the existence of surface vacancies and differences in bond lengths [24]. The large lattice misfit and atomically rough surfaces make MgO very impotent (large ΔT_n) for heterogeneous nucleation of Mg. However, according to Figures 15 and 16, impotent particles promote EGI and enhance grain refinement. This suggests that native MgO particles are highly impotent for heterogeneous nucleation of α-Mg but very suitable for grain refinement of Mg-alloys.

6.3. Addition of More Potent Particles Than Native MgO Will Not Lead to Grain Refinement

In the last 3 decades, there has been a great deal of effort in searching for effective grain refiners for Mg alloys, particularly for Mg-Al-based alloys [13,69,70]. A common approach is to search for potent exogenous particles which can reduce ΔT_n and hence promotes heterogeneous nucleation. However, although the addition of various grain refiners always leads to some degree of grain refinement, none of them is really effective. In fact, they are all less effective than dispersing the MgO films by intensive melt shearing. An interesting fact is that the appropriate incorporation of exogenous particles requires intensive melt stirring, which not only incorporates exogenous particles into the melt but also disperses the MgO films to some extent, leading to some degree of considerable grain refinement. Therefore, it is highly likely that the grain-refining effect comes from the intensive stirring action rather than the exogenous particles. More importantly, the theoretical analysis in this paper provides a clear guideline for the development of grain refiners for Mg alloys.

Figure 19 shows the predicted grain size of Mg-1Al alloy that contains hypothetical nucleant particles of constant number density and size distribution but of varying nucleation potency [20]. Figure 19 suggests that reducing ΔT_n (i.e., increasing particle potency) initially increases grain size and then makes no change in grain size with a further reduction of ΔT_n. This means that the addition of nucleant particles that are more potent than MgO will not lead to further grain refinement. This suggests that all these historical searches for effective grain refiners may have gone in the wrong direction. As will be discussed in the next section, more effective grain refinement of Mg alloys can be achieved by impeding het-

erogeneous nucleation using more impotent particles rather than enhancing heterogeneous nucleation using more potent particles.

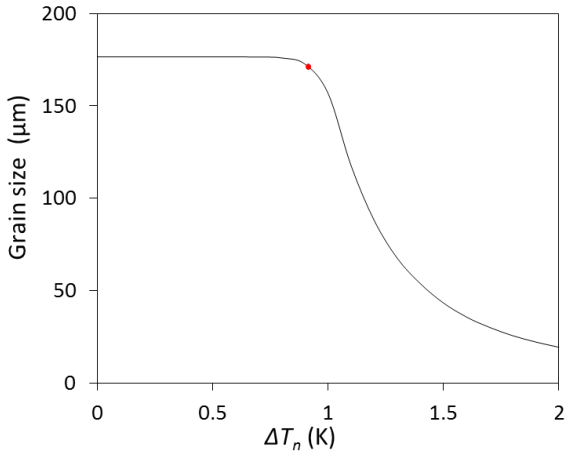

Figure 19. The predicted grain size of Mg-1Al alloy solidified under $\dot{T}$ = 3.5 K/s with nucleant particles with a constant number density ($N_0 = 10^{17}$ m^{-3}) and size distribution (log-normal with d_0 = 0.07 μm and σ = 0.45) but with varying nucleation potency (different ΔT_n) [20]. The red dot marks $N_{PGI} = N_{EGI}$.

6.4. Impeding Nucleation Delivers More Significant Grain Refinement

The traditional approach to grain refiner development is to enhance heterogeneous nucleation by selecting potent nucleant particles. This approach is best demonstrated by the TiB_2-based grain refiners for Al alloys with the following considerations although many of them are not intended historically but because of trial-and-error:

- Native oxide particles in Al alloys, including Al_2O_3, $MgAl_2O_4$ and MgO, are all moderately potent (probably more potent than the bare TiB_2), the grain-refiner particles need to be more potent than the native oxide particles. This is why TiB_2/Al_3Ti-2DC particles are more effective for grain refinement of Al alloys than the bare TiB_2 particles.
- TiB_2 particles themselves are more likely to be less potent than the native oxides. This is why the bare TiB_2 particles are not effective for grain-refining Al alloys.
- The formation of Al_3Ti-2DC on the TiB_2 (0 0 0 1) surface makes the TiB_2/Al_3Ti-2DC particles extremely potent (with a misfit of 0.09%) for heterogeneous nucleation of α-Al [17].
- Properly produced Al-Ti-B grain refiners contain TiB_2 particles with the Al_3Ti-2DC coating and appropriate size distribution and number density.

According to the grain refinement map presented in Figures 15 and 16, the grain refiner particles need to be just more potent than the native particles in order for the grain refiner particles to dominate the heterogeneous nucleation and grain initiation processes, but not more than that.

As we have mentioned previously, the development of grain refiners for Mg alloys has been following the same approach as that for Al alloys but without much real success. This is because such development has not considered the unique characteristics of the native MgO particles in Mg alloys.

One of the most important implications of the grain regimen maps in Figures 15 and 16 is that more significant grain refinement can be achieved by impeding nucleation using impotent particles assuming that there are no more potent particles of significance appearance in the melt [20]. This is demonstrated in Figure 19, which suggests that further grain refinement can be achieved by making the nucleating particles more impotent. In the PGI-dominant zone, grain size is independent of ΔT_n; in the EGI-dominant zone, meanwhile, grain size is reduced significantly with increasing ΔT_n. It is important to note that a prerequisite for this approach is that there are no other particles of significance appearance

in the melt. This new approach has the potential to push grain refinement to a new level unachievable by PGI. Because of the sufficient native oxides in Al and Mg alloys, we can make the best use of such native oxide particles in the alloy melt for more effective grain refinement than chemical inoculation. In this sense, significantly increasing the particle number density and reducing the nucleation potency are two effective approaches to grain refinement of Mg-alloys.

Perhaps the most practical way to implement these new approaches to grain refinement is to make the best use of the native particles already present in the alloy melt. For Mg-alloys, as discussed previously, native MgO particles provide a great opportunity for grain refining Mg-alloys, and intensive melt shearing plays a critical role in making native MgO particles available for grain refinement. As shown in [68,71–74], effective grain refinement can be delivered by intensive melt shearing without any need for grain refiner addition. However, for Al alloys, except for making native particles available for grain refinement, native oxide particles need to be made more impotent to promote EGI for grain refinement. This can be achieved by "poisoning" the native oxides by chemical segregation at the liquid/oxide interface, similar to poisoning TiB_2 particles by co-segregation of Zr and Ti at the liquid/TiB_2 interface [40].

In addition, it is worth noting that grain refinement by native particles is more advantageous than chemical inoculation from the viewpoint of the closed-loop recycling of metallic materials. Chemical inoculation has a low efficiency in adding particles for grain initiation, most of the particles will not initiate grains but segregate at the inter-dendritic regions of the solidified microstructure, having an adverse effect on the mechanical performance. Making native inclusions available for effective grain refinement not only provides more significant grain refinement but also significantly reduces the probability of the existence of large inclusions, having a positive effect on final mechanical performance, such as improved ductility, fatigue strength and fracture toughness. All these factors contribute to the closed-loop recycling of metallic materials.

7. Summary

In this paper, we have briefly reviewed the concept of ESS, which covers prenucleation, heterogeneous nucleation, spherical cap formation, grain initiation and spherical growth. Prenucleation refers to the phenomenon of substrate-induced atomic ordering in the liquid at the liquid/substrate interface as a consequence of structural templating. Prenucleation is affected by temperature, lattice misfit, surface roughness and chemistry, and it provides ultimately a precursor for heterogeneous nucleation at the nucleation temperature. Heterogeneous nucleation is an atomistic process that generates a 2D nucleus at the nucleation temperatures to template further growth. As a deterministic process, heterogeneous nucleation proceeds layer by layer and completes within 3 atomic layers to generate the 2D nucleus, which is a crystal plane of the solid. The specific atomistic mechanisms for generating the 2D nucleus depend on the nature (positive or negative) and the amplitude of the lattice misfit. Following heterogeneous nucleation, the spherical cap formation process can be either constrained or unconstrained depending on the undercooling. A spherical cap can initiate a grain if it can grow beyond a hemisphere, and this grain initiation process is governed by the free growth criterion.

The free growth criterion suggests that grain initiation starts with the largest solid particle followed by progressively smaller solid particles and completes at recalescence. This is called progressive grain initiation (PGI) with a precondition of $\Delta T_n < \Delta T_{gi}(1^{st})$. However, when the nucleant particles are impotent, many solid particles will initiate grains at the nucleation temperature and cause an instantaneous recalescence (i.e., $\Delta T_n = \Delta T_{max}$), and this is called explosive grain initiation (EGI). When the nucleant particles have intermediate potency ($\Delta T_{gi}(1^{st}) < \Delta T_n < \Delta T_{gi}(L^{st})$), the grain initiation process may occur by EGI first followed by PGI, and this is called hybrid grain initiation (HGI). Such grain initiation behaviours can be best described in grain initiation maps, where two characteristic lines representing $\Delta T_n = \Delta T_{gi}(1^{st})$ and $\Delta T_n = \Delta T_{gi}(L^{st})$ divide the $\Delta T_n - \dot{T}$ plot (or $\Delta T_n - C_0$ or

$\Delta T_n - N_0$ plots) into 3 distinctive zones: PGI, EGI and HGI zones. Such grain initiation maps can be used to identify the effects on grain initiation behaviour of factors, such as nucleation potency, particle number density, alloy composition and cooling rate. It has been demonstrated that EGI is favoured by decreasing nucleation potency, cooling rate and solute concentration but increasing particle number density.

Following the grain initiation maps, we introduced the concept of grain refinement maps, where the iso-grain-size lines are used to establish the grain size contour in the $\Delta T_n - \dot{T}$, $\Delta T_n - C_0$ and $\Delta T_n - N_0$ plots. A characteristic line representing $N_{\mathrm{PGI}}/N_{\mathrm{EGI}} = 1$ divides the $\Delta T_n - \dot{T}$ plot (or $\Delta T_n - C_0$ or $\Delta T_n - N_0$ plots) into 2 distinctive zones, PGI-dominant and EGI-dominant. Our theoretical analysis showed that: (1) EGI is more effective for grain refinement than PGI; (2) when grain initiation is fully PGI, grain size decreases with increasing solute concentration, cooling rate and particle number density; (3) when grain initiation is fully EGI, grain size is independent of solute concentration and cooling rate but decreases with increasing particles number density; and (4) when grain initiation is HGI, grain size decreases with increasing solute concentration, cooling rate and particle number density, and the decrease in grain size is more pronounced in the EGI-dominant zone than in the PGI-dominant zone with the increase in particle number density.

When there is more than one type of nucleant particles in an alloy melt, particles will compete not only for heterogeneous nucleation but also for grain initiation. Competition for heterogeneous nucleation is among all available types of nucleant particles. Since heterogeneous nucleation is a deterministic process: It always starts with the particles that have the lowest nucleation undercooling followed by particles with progressively larger nucleation undercooling and finishes at recalescence. Meanwhile, competition for grain initiation is among the solid particles (i.e., nucleant particles that have participated in heterogeneous nucleation). Grain initiation starts with the largest solid particles followed by progressively smaller ones and finishes at recalescence. Grain initiation is dependent on particle size, but independent of types of nucleant particles. The final grain size is a function of the total number of grain initiation events.

The concepts of grain initiation maps and grain refinement maps have a number of practical implications for the grain refinement of metallic materials. Firstly, opposite to the conventional wisdom of grain refinement by enhancing heterogeneous nucleation (reducing ΔT_n) through using potent nucleant particles, the new theory suggests that more significant grain refinement can be achieved by impeding heterogeneous nucleation through deploying impotent particles. This point has been demonstrated by grain refinement of Mg alloys using the native MgO particles which are highly impotent for nucleating α-Mg. Secondly, the new theory suggests that when grain initiation is PGI dominant, the addition of more potent particles as grain refiners will not leads to further reduction of grain size. This has explained why the search for grain refiners for Mg-alloys has not been successful. Thirdly, native oxides, in both Al and Mg alloys, have the potential to be made effective for grain refinement without the need for chemical inoculation. This is particularly desirable for closed-loop recycling of metallic materials. Finally, the new theory can be used as a guideline for manipulating nucleation potency of selected nucleant particles for effective nucleation control through deliberate chemical segregation at the liquid/substrate interface.

Author Contributions: Z.F.: conceptualization, methodology, writing—review and editing, project administration, funding acquisition; F.G.: investigation, data curation, formal analysis, visualization, writing—original draft preparation. All authors have read and agreed to the published version of the manuscript.

Funding: This work was financially supported by the EPSRC (UK) under grant number EP/N007638/1.

Institutional Review Board Statement: Not applicable.

Informed Consent Statement: Not applicable.

Data Availability Statement: Not applicable.

Conflicts of Interest: The authors declare no conflict of interest.

References

1. McCartney, D.G. Grain refining of Al and its alloys using inoculants. *Int. Mater. Rev.* **1989**, *34*, 247–260. [CrossRef]
2. Easton, M.; StJohn, D. Grain refinement of aluminum alloys: Part I. the nucleant and solute paradigms-a review of the literature. *Metall. Mater. Trans. A* **1999**, *30*, 1613–1623. [CrossRef]
3. Murty, B.; Kori, S.A.; Chakraborty, M. Grain refinement of aluminium and its alloys by heterogeneous nucleation and alloying. *Int. Mater. Rev.* **2002**, *47*, 3–29. [CrossRef]
4. Greer, A.L. Overview: Application of heterogeneous nucleation in grain-refining of metals. *J. Chem. Phys.* **2016**, *145*, 211704. [CrossRef] [PubMed]
5. Easton, M.; Qian, M.; Prasad, A.; StJohn, D. Recent advances in grain refinement of light metals and alloys. *Curr. Opin. Solid State Mater. Sci.* **2016**, *20*, 13–24. [CrossRef]
6. Gibbs, J.W. On the equilibrium of heterogeneous substances. *Am. J. Sci.* **1879**, *16*, 441–458. [CrossRef]
7. Volmer, M.; Weber, A.Z. Nucleus formation in supersaturated systems. *Z. Phys. Chem.* **1926**, *119*, 277–301. [CrossRef]
8. Becker, R.; Döring, W. Kinetic treatment of nucleation in supersaturated vapors. *Ann. Phys.* **1935**, *24*, 719–752. [CrossRef]
9. Zeldovich, J.B. On the theory of new phase formation: Cavitation. *Acta Physicochim. USSR* **1943**, *18*, 1–22.
10. Turnbull, D. Kinetics of heterogeneous nucleation. *J. Chem. Phys.* **1950**, *18*, 198–203. [CrossRef]
11. Turnbull, D. Kinetics of solidification of supercooled liquid mercury droplets. *J. Chem. Phys.* **1952**, *20*, 411–424. [CrossRef]
12. Kelton, K.F.; Greer, A.L. *Nucleation in Condensed Matter: Applications in Materials and Biology*; Pergamon: Oxford, UK, 2010.
13. Ali, Y.; Qiu, D.; Jiang, B.; Pan, F.; Zhang, M.-X. Current research progress in grain refinement of cast magnesium alloys: A review article. *J. Alloys Compd.* **2015**, *619*, 639–651. [CrossRef]
14. Zhang, M.-X.; Kelly, P.M.; Easton, M.A.; Taylor, J.A. Crystallographic study of grain refinement in aluminum alloys using the edge-to-edge matching model. *Acta Mater.* **2005**, *53*, 1427–1438. [CrossRef]
15. Fu, H.; Qiu, D.; Zhang, M.; Wang, H.; Kelly, P.; Taylor, J. The development of a new grain refiner for magnesium alloys using the edge-to-edge model. *J. Alloys Compd.* **2008**, *456*, 390–394. [CrossRef]
16. Jiang, B.; Qiu, D.; Zhang, M.X.; Ding, P.D.; Gao, L. A new approach to grain refinement of an Mg-Li-Al cast alloy. *J Alloys Compd.* **2010**, *492*, 95–98. [CrossRef]
17. Fan, Z.; Wang, Y.; Zhang, Y.; Qin, T.; Zhou, X.R.; Thompson, G.E.; Pennycook, T.; Hashimotob, T. Grain refining mechanism in the Al/Al-Ti-B system. *Acta Mater.* **2015**, *84*, 292–304. [CrossRef]
18. Fan, Z.; Gao, F.; Wang, Y.; Men, H.; Zhou, L. Effect of solutes on grain refinement. *Prog. Mater. Sci.* **2022**, *123*, 100809. [CrossRef]
19. The Future Liquid Metal Engineering Hub: Report (2015–2021). Available online: https://www.lime.ac.uk/blog/2021-annual-report-published (accessed on 4 October 2022).
20. Fan, Z.; Gao, F.; Jiang, B.; Que, Z. Impeding nucleation for more significant grain refinement. *Sci. Rep.* **2020**, *10*, 9448. [CrossRef]
21. Men, H.; Fan, Z. Prenucleation induced by crystalline substrates. *Metall. Mater. Trans. A* **2018**, *49*, 2766–2777. [CrossRef]
22. Jiang, B.; Men, H.; Fan, Z. Atomic ordering in the liquid adjacent to an atomically rough solid surface. *Comput. Mater. Sci.* **2018**, *153*, 73–81. [CrossRef]
23. Fang, C.M.; Men, H.; Fan, Z. Effect of substrate chemistry on prenucleation. *Metall. Mater. Trans. A* **2018**, *49*, 6231–6242. [CrossRef]
24. Fang, C.M.; Fan, Z. Prenucleation at the interface between MgO and liquid magnesium: An ab initio molecular dynamics study. *Metall. Mater. Trans. A* **2020**, *51*, 788–797. [CrossRef]
25. Fang, C.M.; Fan, Z. Prenucleation at the liquid-Al/α-Al_2O_3 and the liquid-Al/MgO interfaces. *Comp. Mater. Sci.* **2020**, *171*, 109258. [CrossRef]
26. Fang, C.M.; Fan, Z. Atomic ordering at the liquid-Al/$MgAl_2O_4$ interfaces from ab initio molecular dynamics simulations. *Metall. Mater. Trans. A* **2020**, *51*, 6318–6326. [CrossRef]
27. Fang, C.; Yasmin, S.; Fan, Z. Interfacial interaction and prenucleation at liquid-Al/γ-Al_2O_3 {1 1 1} interfaces. *J. Phys. Comm.* **2021**, *5*, 015007. [CrossRef]
28. Men, H.; Fang, C.; Fan, Z. Prenucleation at the liquid/substrate interface: An overview. *Metals* **2022**, *12*, 1704. [CrossRef]
29. Fan, Z. An epitaxial model for heterogeneous nucleation on potent substrates. *Metall. Mater. Trans. A* **2013**, *44*, 1409–1418. [CrossRef]
30. Fan, Z.; Men, H. A molecular dynamics study of heterogeneous nucleation in generic liquid/substrate systems with positive lattice misfit. *Mater. Res. Express* **2020**, *7*, 126501. [CrossRef]
31. Fan, Z.; Men, H.; Wang, Y.; Que, Z. A new atomistic mechanism for heterogeneous nucleation in the systems with negative lattice misfit: Creating a 2D template for crystal growth. *Metals* **2021**, *11*, 478. [CrossRef]
32. Fan, Z.; Men, H. An overview on atomistic mechanisms of heterogeneous nucleation. *Metals* **2022**, *12*, 1547. [CrossRef]
33. Fan, Z.; Men, H. Heterogeneous nucleation and grain initiation on a single substrate. *Metals* **2022**, *12*, 1454. [CrossRef]
34. Fan, Z. Heterogeneous nucleation, grain initiation and grain refinement of Mg-Alloys. In Proceedings of the 11th International Conference on Magnesium Alloys and Their Applications, Beaumont Estate, Old Windsor, UK, 24–27 July 2018; pp. 7–17.
35. Fan, Z.; Lu, S.Z. A simple model for spherical growth in alloy solidification. *IOP Conf. Ser. Mater. Sci. Eng.* **2016**, *117*, 012016. [CrossRef]
36. Yonemura, M.; Osuki, T.; Terasaki, H.; Komizo, Y.; Sato, M.; Kitano, A. In-situ observation for weld solidification in stainless steels using time-resolved X-ray diffraction. *Mater. Trans.* **2006**, *47*, 310–316. [CrossRef]

37. Yonemura, M.; Osuki, T.; Terasaki, H.; Komizo, Y.; Sato, M.; Toyokawa, H. Two-dimensional time-resolved X-ray diffraction study of directional solidification in steels. *Mater. Trans.* **2006**, *47*, 2292–2298. [CrossRef]
38. Yonemura, M.; Osuki, T.; Terasaki, H.; Komizo, Y.; Sato, M.; Toyokawa, H.; Nozaki, A. Two-dimensional time-resolved x-ray diffraction study of dual phase rapid solidification in steels. *J. Appl. Phys.* **2010**, *107*, 013523. [CrossRef]
39. Wang, Y.; Wang, S.; Que, Z.; Fang, C.; Hashimoto, T.; Zhou, X.; Ramasse, Q.M.; Fan, Z. Manipulating nucleation potency of substrates by interfacial segregation: An overview. *Metals* **2022**, *12*, 1636. [CrossRef]
40. Wang, Y.; Fang, C.; Zhou, L.; Hashimoto, T.; Zhou, X.; Ramasse, Q.; Fan, Z. Mechanism for Zr poisoning of Al-Ti-B based grain refiners. *Acta Mater.* **2019**, *164*, 428–439. [CrossRef]
41. Greer, A.L.; Bunn, A.M.; Tronche, A.; Evans, P.V.; Bristow, D.J. Modelling of inoculation of metallic melts: Application to grain refinement of Al by Al-Ti-B. *Acta Mater.* **2000**, *48*, 2823–2835. [CrossRef]
42. Cantor, B. Heterogeneous nucleation and adsorption. *Philos. Trans. R. Soc. Lond. Ser. A Math. Phys. Eng. Sci.* **2003**, *361*, 409–417. [CrossRef]
43. Young, T. III. An essay on the cohesion of fluids. *Philos. Trans. R. Soc. Lond.* **1805**, *95*, 65–87. [CrossRef]
44. Kim, W.; Cantor, B. Solidification behaviour of Pb droplets embedded in a Cu matrix. *Acta Metall. Mater.* **1992**, *40*, 3339–3347. [CrossRef]
45. Kim, W.; Cantor, B. Heterogeneous nucleation of Al_2Cu in Al-Cu eutectic liquid droplets embedded in an al matrix. *Acta Metall. Mater.* **1994**, *42*, 3045–3053. [CrossRef]
46. Turnbull, D.; Vonnegut, B. Nucleation catalysis. *Ind. Eng. Chem.* **1952**, *44*, 1292–1298. [CrossRef]
47. Quested, T.; Greer, A. The effect of the size distribution of inoculant particles on as-cast grain size in aluminium alloys. *Acta Mater.* **2004**, *52*, 3859–3868. [CrossRef]
48. Van Ende, M.-A.; Guo, M.; Zinngrebe, E.; Blanpain, B.; Jung, I.-H. Evolution of non-metallic inclusions in secondary steelmaking: Learning from inclusion size distributions. *ISIJ Int.* **2013**, *53*, 1974–1982. [CrossRef]
49. Fan, Z.; Gao, F.; Zhou, L.; Lu, S.Z. A new concept for growth restriction during solidification. *Acta Mater.* **2018**, *152*, 248–257. [CrossRef]
50. Men, H.; Jiang, B.; Fan, Z. Mechanisms of grain refinement by intensive shearing of AZ91 alloy melt. *Acta Mater.* **2010**, *58*, 6526–6534. [CrossRef]
51. Wang, Y.; Fan, Z.; Zhou, X.; Thompson, G. Characterisation of magnesium oxide and its interface with α-Mg in Mg–Al-based alloys. *Philos. Mag. Lett.* **2011**, *91*, 516–529. [CrossRef]
52. Wang, S.; Wang, Y.; Ramasse, Q.; Fan, Z. The nature of native MgO in Mg and its alloys. *Metall. Mater. Trans. A* **2020**, *51*, 2957–2974. [CrossRef]
53. Peng, G.S.; Wang, Y.; Fan, Z. Competitive heterogeneous nucleation between Zr and MgO particles in commercial purity magnesium. *Metall. Mater. Trans. A* **2018**, *49*, 2182–2192. [CrossRef]
54. Gao, F.; Fan, Z. Competition for nucleation and grain initiation during solidification. *Metals* **2022**, *12*, 1512. [CrossRef]
55. Cui, X.; Wu, Y.; Gao, T.; Liu, X. Preparation of a novel Al–3B–5Sr master alloy and its modification and refinement performance on A356 alloy. *J. Alloys Compd.* **2014**, *615*, 906–911. [CrossRef]
56. Wang, T.; Chen, Z.; Fu, H.; Xu, J.; Fu, Y.; Li, T. Grain refining potency of Al–B master alloy on pure aluminum. *Scr. Mater.* **2011**, *64*, 1121–1124. [CrossRef]
57. Bolzoni, L.; Babu, N.H. Towards industrial Al-Nb-B master alloys for grain refining Al-Si alloys. *J. Mater. Res. Technol.* **2019**, *8*, 5631–5638. [CrossRef]
58. Zhao, C.; Li, Y.; Xu, J.; Luo, Q.; Jiang, Y.; Xiao, Q.; Li, Q. Enhanced grain refinement of Al-Si alloys by novel Al-V-B refiners. *J. Mater. Sci. Technol.* **2021**, *94*, 104–112. [CrossRef]
59. Chang, W.; Shen, Y.; Su, Y.; Zhao, L.; Zhang, Y.; Chen, X.; Sun, M.; Dai, J.; Zhai, Q. Grain refinement of AZ91 magnesium alloy induced by Al-V-B master alloy. *Metals* **2019**, *9*, 1333. [CrossRef]
60. Liao, H.; Zhan, M.; Li, C.; Ma, Z.; Du, J. Grain refinement of Mg-Al alloys inoculated by $MgAl_2O_4$ powder. *J. Magnes. Alloy.* **2021**, *9*, 1211–1219. [CrossRef]
61. Zhang, J.; Zhou, G.; Jiang, B.; Luo, A.; Zhao, X.; Tang, A.; Pan, F. A novel Mg-CaMgSn master alloy for grain refinement in Mg-Al-based alloys. *Metals* **2021**, *11*, 1722. [CrossRef]
62. Fan, W.; Bai, Y.; Zuo, G.; Hao, H. The control of NbB_2 particles in Al-NbB_2 master alloy and its effect on grain refinement of AZ91 magnesium alloy. *Mater. Sci. Eng. A* **2022**, *854*, 143808. [CrossRef]
63. Fan, W.; Bai, Y.; Li, J.; Li, G.; Hao, H. Grain refinement of Mg-Al alloys by a new Al-4.1V-1.7B refiner containing sole VB_2 particles. *J. Mater. Eng. Perform.* **2022**, 1–12. [CrossRef]
64. Zhou, L.; Gao, F.; Peng, G.; Alba-Baena, N. Effect of potent TiB_2 addition levels and impurities on the grain refinement of Al. *J. Alloys Compd.* **2016**, *689*, 401–407. [CrossRef]
65. Gao, F.; Fan, Z. Effect of nucleant particle agglomeration on grain size. *Metall. Mater. Trans. A* **2022**, *53*, 810–822. [CrossRef]
66. Sin, S.L.; Elsayed, A.; Ravindran, C. Inclusions in magnesium and its alloys: A review. *Int. Mater. Rev.* **2013**, *58*, 419–436. [CrossRef]
67. Bakke, P.; Karlsen, D.O. Inclusion assessment in magnesium and magnesium base alloys. *SAE Trans.* **1997**, *106*, 314–326. [CrossRef]

68. Fan, Z.; Wang, Y.; Xia, M.; Arumuganathar, S. Enhanced heterogeneous nucleation in AZ91D alloy by intensive melt shearing. *Acta Mater.* **2009**, *57*, 4891–4901. [CrossRef]
69. StJohn, D.H.; Easton, M.; Qian, M.; Taylor, J.A. Grain refinement of magnesium alloys: A review of recent research, theoretical developments, and their application. *Metall. Mater. Trans. A* **2012**, *44*, 2935–2949. [CrossRef]
70. Karakulak, E. A review: Past, present and future of grain refining of magnesium castings. *J. Magnes. Alloy.* **2019**, *7*, 355–369. [CrossRef]
71. Tzamtzis, S.; Zhang, H.; Babu, N.H.; Fan, Z. Microstructural refinement of AZ91D die-cast alloy by intensive shearing. *Mater. Sci. Eng. A* **2010**, *527*, 2929–2934. [CrossRef]
72. Patel, J.B.; Lloyd, P.; Peng, G.; Fan, Z. Development of the new high shear technology for continuous processing of Mg-alloys for ingot casting. In *Magnesium Technology*; Singh, A., Solanki, K., Manuel, M.V., Neelameggham, N.R., Eds.; Springer: Cham, Switzerland, 2016; pp. 29–33.
73. Zuo, Y.B.; Jiang, B.; Zhang, Y.; Fan, Z. Grain refinement of DC cast magnesium alloys with intensive melt shearing. *IOP Conf. Ser. Mater. Sci. Eng.* **2012**, *27*, 012043. [CrossRef]
74. Patel, J.B.; Yang, X.; Mendis, C.L.; Fan, Z. Melt conditioning of light metals by application of high shear for improved microstructure and defect control. *JOM* **2017**, *69*, 1071–1076. [CrossRef]